Paper 1: Fluid induced multistage recrystallisation microstructures in Quartzites and Quartz veins from the Bamble shear zone complex

Bjørn Eske Sørensen
Department of Geology and Mineral Resources Engineering, Norwegian University of Science and Technology (NTNU), N7491 Trondheim, Norway
(bjorn.soresen@ntnu.no)

Rune Berg Larsen
Department of Geology and Mineral Resources Engineering, Norwegian University of Science and Technology (NTNU), N7491 Trondheim, Norway
(rune.larsen@ntnu.no)

Abstract

The Bamble sector contains abundant coarse-grained quartzites that experienced Sweconorwegian high grade metamorphism. This study concerns quartzites from the Nidelva Quartzite Complex close to Blakstad. Static high grade textures formed at peak conditions (750°C/6-7 kbar (Nijland and Maijer, 1993)), are cut by younger localized high-grade shear zones with mm-sized amoeboid quartz grains. Localized retrogression related to the formation of white mica occurs throughout the area, typically related to mm-thin fault zones with adjacent SGR (subgrain rotation recrystallisation) causing a reduction in grain size (50-200 microns)

Four quartz types were defined with the SEM-CL technique:

Qz1: Bright islands demarcated by darker cracks. Typically they are partially luminescence quenched. The bright islands in Qz1 relate to the high grade history of the area, but the cracking relates to retrogression and formation of Qz2 (next).

Qz2: Light grey, sometimes featuring weak oscillatory zonation. Qz2 has brighter cores and darker rims approaching the luminescence of Qz3. The formation of the island texture in Qz1 and Qz2 are probably related, since Qz2 and the cracks in Qz1 has the same luminescence.

Qz3: Dark grey diffuse fluid channel textures, which follow grain boundaries or intersect grains. Qz3 relates to alteration of biotite to muscovite and SGR in narrow fault zones.

Qz4. Narrow cracks and pods of black quartz, intersecting all other qz-types.

Fluid inclusions related to Qz1, Qz2 and Qz3 are absent or very tiny in the quartzites, but quartz veins in amphibolite carry fluid inclusions that may be related to the same quartz types as those found in the quartzites. The fluids follow the textural evolution of quartz. Qz1 relates to CO_2 rich LV fluids, Qz2 to potassic alteration of amphibolite and coexisting low salinity CO_2-rich H_2O-CO_2 and brine CO_2-H_2O-(Na,K)Cl LV fluids. Qz3 relates to brine (Na,Ca)Cl-H_2O LVS fluids and scapolitisation of amphibolite (see paper 2, Sørensen and Larsen, 2007).

Trace element contents in quartz measured by LA-HR-ICP-MS relate both to the textural and fluid evolution. Qz1 is enriched in B, Al and Ti when compared with the other types. Qz2 has low Al contents (<50 ppm) but variable Ti contents in quartz veins in amphibolite (210-10 ppm) due to inclusions of rutile needles and more consistent values in quartzites (peak value 32 ppm). Qz3 has Ti< 5 ppm and Al contents below 10 ppm and low B.

The textural and chemical evolution of quartz is explained by two major influxes of aqueous fluids during regional uplift and retrogression. They caused recrystallisation in the otherwise dry high grade quartzites. The first introduction of aqueous fluids was associated with brecciation of the high grade quartz (Qz1) and dissolution/precipitation of quartz (Qz2). Ti in quartz thermometry (Wark and Watson, 2006) of this stage gives 626°C in agreement with a retrograde PT-path deduced from phase diagrams (paper 2, Sørensen and Larsen, 2007). During subsequent deformation, Qz2 deformed more plastically than Qz1, probably due to an increase in the H_2O fugacity. Later fluid influx, related to scapolitisation of amphibolite was associated with localized recrystallisation (Qz3) and alteration of biotite to muscovite. During subsequent deformation, Qz3 deformed plastically and recovered by SGR, resulting in a reduction of grain size, whereas Qz1 quartz formed micro faults. Qz2 was plastic but did not experience SGR to the same degree as Qz3 quartz. Increased plasticity and recovery rates most likely relate to an increased water/rock ratio as also documented by fluid inclusions (paper 2, Sørensen and Larsen, 2007). However atomic lattice distortion by trace elements may also obstruct dislocation climb hence recovery and strain softening processes.

Key words:

Fluid migration patterns, shear zone fluids, Quartz, retrograde recrystallisation of quartz, high purity quartz, metasomatism, Ti-mobilization, Hydrolytic weakening, scapolitisation, biotite-alteration, rose quartz, dumortierite

1 Introduction

The purpose of the current study was to better understand the retrograde behaviour of high grade quartz and quartzites under the influence of infiltrating fluids and shear zone deformation. Furthermore, to study if quartzitic lithologies, due to their relatively simple chemistry and high preservation rate, may provide new information on fluid

migration and regional mass balance properties during shear zone processes. Both chemical and rheological aspects were considered. In the literature a connection between shear zones, fluids and regional mass transfer was often suggested, particularly in connection with auriferous ore deposits (e.g. Cameron, 1993; Cameron et al., 1993; Colivine et al., 1984; Groves et al., 1992; McCuaig and Kerrich, 1998; Nesbit and Muehlenbachs, 1989; Nesbit et al., 1986; Sibson et al., 1988). However the properties of fluid migration patterns are normally not explained in satisfactory details.

In this paper we present documentation of fluid migration and fluid induced multi stage recrystallisation in quartzites from the Bamble sector. This mega shear zone is well known for its regional fluid infiltration phenomena, a process which is particularly well described for the early high grade part of the history (see geological setting in the next section.). In classic metamorphic petrology studies, quartzites are normally excluded, because they usually lack metamorphic index assemblages. However quartzite features some unique abilities that are not common in other metamorphic lithologies. Particularly their simple chemistry being almost pure SiO_2 preserves evidence for mass balance relations. Accordingly, small proportions of added or removed material are easily recorded, for example in new mineral assemblages. Secondly quartz, the main mineral in quartzites is a good preservative for paleofluids in fluid inclusions, and is used to investigate fluids in many silica saturated rocks. Furthermore, quartz is stable throughout most crustal conditions whereas other minerals may come and go according to their thermodynamic properties. Accordingly early metamorphic/metasomatic event that are lost to decomposition of the index mineral may very well be preserved by remnants of quartz. Finally, quartz is an important commodity in the production of silica glasses and silicon product including high purity solar cell silicon that is currently in high demand by the world marked. The current study throws new light of natural refinement processes promoting the genesis of high purity quartz in the nature.

Our study relies on SEM-CL to interpret the complex recrystallisation behaviour observed in quartzites, quartz rich gneisses and quartz veins from the Bamble sector. The aim is to understand the parameters that control rheological and chemical behaviour of quartz during uplift and to understand their effects on lithological properties. SEM-CL has the advantage that it is imaging defect structures. However the intensity of the SEM-CL signal alone does not give direct evidence of the trace element concentrations because the CL signal reflects structural defects and not all defects are related to trace elements.

2 Previous work

Under upper crustal conditions, quartzites are some of the softest rocks in the continental crust hence may work as decollement zones during tectonic events (e.g. Tullis, 2002). However, contrary to the results of numerous quartz deformation experiments (e.g. Griggs and Blacic, 1965; Kronenberg, 1994; Kronenberg et al., 1986;

Post and Tullis, 1998) it is often neglected, that different quartz types has different rheological properties. Tullis and Yund (1989) and Post et al. (1996) studied the effects of water and pressure on the recovery rate in deforming quartz aggregates and found a good correlation between f_{H_2O} and the lowering of plastic strength. Post et al. (1996) evaluated several parameters in their experiments (a_{H^+}, f_{H_2O}; a_{OH^-}) and concluded that only H_2O had significant effects on creep strength as well as annealing rate. Both strain induced grain boundary migration and dislocation climb is enhanced by H_2O. Thus H_2O promotes recrystallisation accommodated dislocation creep as well as climb accommodated creep (Post et al., 1996). Kohlstedt and co-workers (1995) suggested the following formulation of the effect of H_2O in the flow law of quartz:

$$\dot{\varepsilon} = A\sigma^n f_{H_2O}{}^m e^{-(Q/RT)}$$

At constant strain rate and temperature the f_{H_2O} exponent can be determined from

$$\frac{d\log\sigma}{d\log(f_{H_2O})} = -\frac{m}{n}$$

$\dot{\varepsilon}$ is the strain rate, A a material constant, σ the differential stress, Q the activation energy, R the gas constant, T the temperature in K, m the f_{H_2O} fugacity exponent and n is the stress exponent.

The reliability of this expression was confirmed by Post and co-workers (1996), though the m exponent should be determined in steady state creep with free H_2O present and one deformation mechanism must dominate. Therefore, uncertainties may be introduced because the H_2O fugacity also increase climb rates significantly, causing deformation mechanism to change e.g. from dislocation glide to dislocation creep (Post and Tullis, 1998).

The rate H_2O incorporation into quartz from a coexisting fluid is approximately an order of magnitude larger than the experimentally determined rate of oxygen diffusion (Post and Tullis, 1998). By assuming that the grain boundary diffusion is infinite Post & Tullis (1998) simulated the number of years it would take different grain sizes to re-equilibrate with the ambient H_2O fugacity. Their results imply that all grain sizes from 10 microns to 1 mm would re-equilibrate within 1 Ma at T>450°C, whereas at 300-350°C large grain sizes would require re-equilibration times >100 Ma., i.e. much longer than normally assumed residence times during uplift. Accordingly, in amphibolite facies, if fluids are present, quartzites should re-equilibrate at the cm-dm scale with the ambient water fugacity within some millions of years whereas quartzites, in the greenshist facies, would only re-equilibrate at the micrometer scale in the same time span. Because fluids migrate in pulses in the crust they are not residing throughout the metamorphic history. Accordingly, rocks in the amphibolite facies may be in disequilibrium at ambient H_2O fugacity.

The experimental results on hydrolytic weakening in quartzites correlate well with observations in natural quartz tectonites. Muto and co-workers (2004) showed that

there was a good correlation between decreasing grain size in quartz in a natural shear zone and molecular H_2O, SiOH and SiH groups. The relation between H_2O fugacity and recrystallisation is complex. Muto and co-workers (2005), however, found that the integrated H_2O IR spectra dropped along with increasing shear strain and recrystallisation in a high strain shear zone. This drop in the water content followed a drop in the SEM-CL intensity. It was concluded that dynamic recrystallisation lead to the removal of H_2O from quartz and that the main luminescence in the quartz comes from H_2O related defects (Muto et al., 2005). However numerous studies document a relation between CL and trace elements other than water in quartz hence contradicting the conclusions of Muto (2005) (e.g. .Goetze, 2000; Goetze et al., 2004; Goetze et al., 2005; Goetze et al., 2001; Müller et al., 2003). In these studies, colour CL and spectroscopy is used in combination with other analytical techniques documenting defect centres in the quartz lattice via e.g. EPR (electron paramagnetic resonance) and comparing with CL-spectra recorded under controlled conditions.

Landtwing and Pettke (2005) documented a positive correlation between TE content in hydrothermal quartz and the intensity in grey scale SEM-CL images. Van den Kerkhof et al (2004), documented fluid related recovery by SEM-CL imaging and spectroscopy in dispersed veins in enderbitic charnokite in the proximity of the area addressed in our study. They found a correlation between a drop in luminescence and mainly Ti-defects in the quartz.

3 Geological setting

The Bamble sector comprises exceptionally well preserved high grade amphibolite-granulite facies rocks. Most authors agree that the peak PT-conditions were approximately 850 °C in the HT granulite facies zone at Arendal, and tapering towards lower T in a thermal dome pattern (Figure 1). Peak P conditions were roughly 6-7 kb.

Fluid inclusion studies documented CO_2 dominated fluids in amphibolite lithologies, and CO_2 + brines in more siliceous gneisses (Touret, 1971). This COH fluid composition is matched by fluid modelling using the iron-titanium oxygen barometer (Harlov, 2000). The conditions during exhumation are far less constrained although the absence of retrograde aluminous silicate assemblages imply high alkali-chloride activities in the retrograde fluids (Touret, 1968). Knudsen (1996) summarise the available retrograde PT-paths of the Bamble sector and conclude that the PT-paths display systematic spatial variations characterised by a steep retrograde path in the southernmost part (Knudsen, 1996), followed by isobaric cooling in the southeast and a slight pressure increase in the north. However, it is also concluded that the P-T estimates are uncertain.

Sørensen and Larsen (2007, paper 2) used their observations in calcsilicate rocks along with fluid inclusion data and mineral paragenetic data of Nijland and co-workers (1993a) to redefine the cooling and uplift path of the Froland area. Their results imply a four stage PT-X_{fluid} cooling and uplift path:

1. Approximately at 626°C and 7 kb. The total fluid composition for this stage is in mole fractions: XCO_2 = 0.30, XH_2O = 0.62, XNaCl = 0.08 (30 wt% NaCl in the aqueous phase). Because sanidine + tremolite is not replaced by phlogopite + calcite + quartz during cooling and uplift we infer that XCO_2 decreased rapidly with falling temperatures.
2. Sørensen and Larsen (2007, paper 2) infer a shift from potassic-sodic and sodic-calcic alteration based on the assemblages documented by (Nijland et al., 1993a). MII (kyanite-chlorite-muscovite veins) and MIII (margarite + corundum) of (Nijland et al., 1993a) have overlapping PT stability fields. Both are alteration products of an assemblage originally comprising corundum + plagioclase. MII muscovite was stabilised by potassium rich fluids. Decreased potassium content/increased calcium content of the fluid stabilised margarite over muscovite and formed the margarite + corundum assemblage. P-T conditions of MII represent a relatively narrow temperature field from 450 to 550°C. Pressure is constrained by the stability of kyanite which defines the lower pressure limit to 4.5 kb.
3: The uplift path is constrained by the isochore of fluid inclusions in quartz (FIA3 of Sørensen and Larsen, (2007, paper 2). The well preserved fluid inclusions suggest an uplift path that was sub parallel with the isochore. Uplift occurred at 300 to 400°C. Accordingly, the Froland lithologies experienced a P-drop from 5-7 kb to 2-3 kb at 100 °C lower T than the interpretation provided by Nijland et al.(1993a).
4: Post kinematic alteration during final cooling after exhumation, including vug assemblages comprising epidote-calcite-actinolite-pyrite (paper 2, Sørensen and Larsen, 2007) and coexisting prehnite-pumpelyite + fluid inclusions at 2-3 kb and 175-280°C (Nijland et al., 1993a; Touret and Olsen, 1985).

Fluid related alteration follows a rhombohedral net work of shear zones and faults, associated with exhumation and possibly also extensional collapse of the Sweconorwegian mountain range. Brine-rich fluid inclusions are documented together with the alteration assemblages (e.g. Nijland and Touret, 2001; Nijland et al., 1998; Sørensen and Larsen, 2007; Touret, 1985).

Quartzites and quartz rich gneisses are abundant in the Bamble Sector. Most of the work on Quartz rich rocks is focused on sedimentary structures and chemistry and not the metamorphic recrystallisation. There are several compositional and textural types including very pure and coarse-grained quartzite, quartzo-feldspatic gneiss and nodular gneiss/quartzite. The quartztose rocks contain variable amounts of tourmaline. Layers of stratabound tourmaline are locally observed (Nijland et al., 1993b). Black tourmaline frequently occur on the more Al-rich cleavage planes ((Nijland et al., 1993b); this study). Red-brown transparent tourmaline (field colour, orange-red brown in thin section, Dravitic) occurs in layers and lenses in quartz microcline and oligoclase and biotite at Grendal Tjern (Nijland et al., 1993b) and at Trevann (This study). Black tourmaline (field colour, green-brown pleocroic in thin section Schorl-Dravite) also occur as reaction zones bordering quartz veins in quartzites together with biotite and muscovite. In addition black (Schorl rich) and brown (Drawite rich) tourmaline together with biotite defines the foliation in some mylonitic gneisses. Rare sedimentary

structures occur in the Nidelva Quartzite Complex (NQC), and well documented cases of cross beddings, mud cracks, ripple marks and strongly deformed meta-conglomerates imply a sedimentary origin (Nijland et al., 1993b).

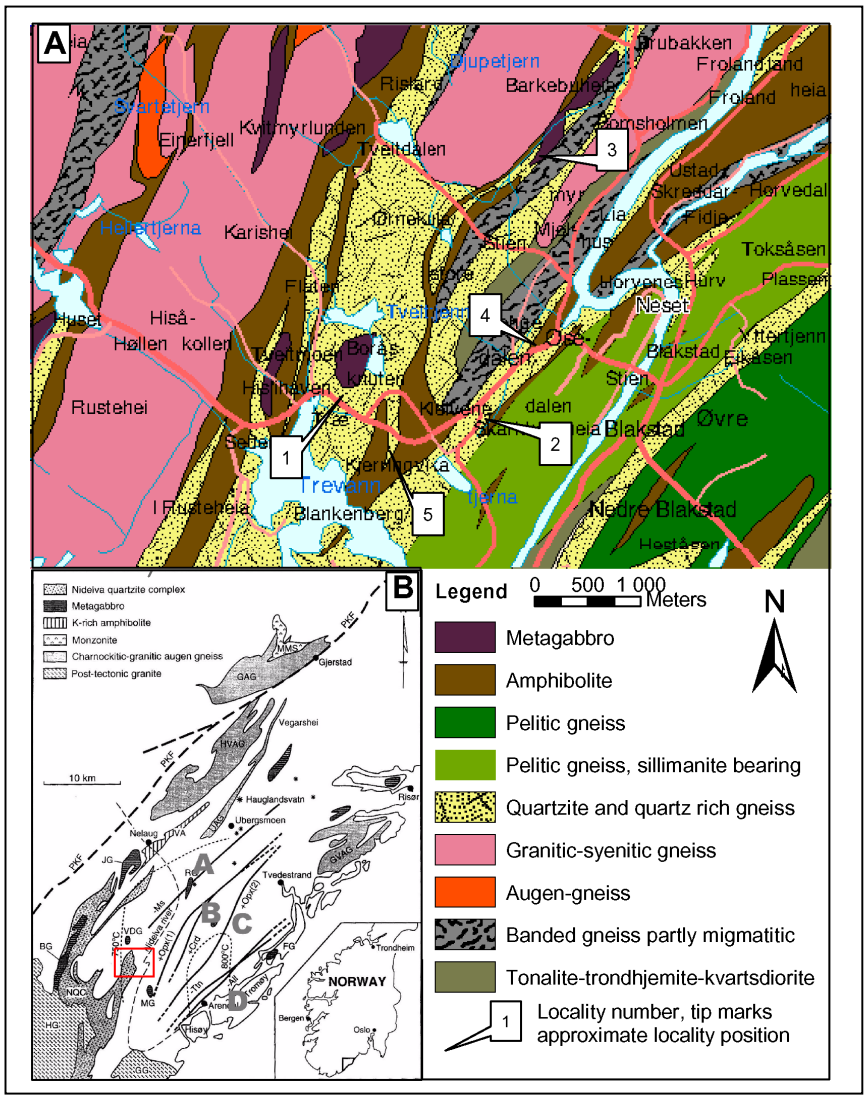

Figure 1: Geological maps. A) Detailed map of the investigated area. Modified from Geological Survey of Norway N-50 berggrunns kart 16123 Nelaug and 16114 Arendal. Geographic data (roads, lakes and rivers) are added for easy orientation (source: www.geonorge.no). B) Overview map of the Bamble Sector displaying the most important rock units (see legend on map). Insert show the position of the Bamble Sector in South

Norway. Red square denotes the position of the study area shown in A. From Nijland et al. (1998). Also shown in B are the metamorphic zones in the Bamble Sector.

4 Methodology

4.1 Sample preparation

The textural relations between the different quartz types are typically found in a single hand specimen. Samples of quartzite dominated by the individual types were also included, but samples displaying all types and textural relations were prioritised. Many samples were cut and polished roughly, before they were scanned on wet transparencies. Scanned pictures of rock slices of the selected hand specimens uncovered the timing and spatial relations between the different quartzite textures (see for example Figure 2). Based on these observations thin sections were prepared.

Thin and thick sections (for LA-ICP-MS) were prepared from the same block, in order to correlate common textures. Thick sections for LA-ICP-MS had to be 200 µm to accommodate the ablation craters for the ICP_MS analysis (up to 90 microns). Therefore, optical microstructures in the quartz were almost impossible to infer from the thick sections alone and were made in combination with observations in the thin sections. The quality of polishing is essential for the quality of SEM-CL imaging

4.2 SEM-CL methodology

SEM-CL was performed on a low vacuum SEM at the Department of Materials Sciences, NTNU. The luminescence signal was collected with a Robinson detector, giving a greyscale picture. Samples with much K-feldspar were avoided because high luminescence of the latter clouded the signal from quartz.

The absolute intensity could not be used as a criterion of distinction between quartz types because the contrast and intensity setting had to be changed continuously to enhance textural features. A mosaic of images was recovered and sample in a single picture, in some cases covering the entire thin sections. In most cases the minimum working distance of 20 mm was chosen to achieve the best possible signal, but to take pictures at lower magnifications sometimes a working distance of 30 or 40 mm were used in combination with details from selected areas at 20 mm working distance. The acceleration voltage was also varied in order to optimise the image. For bigger working distances (20 or 40 mm) an acceleration voltage of 30 KV was optimal, whereas 15-25 KV was sufficient for working distance of 20 mm. Good polishing is essential to the quality of the SEM-CL imaging, and it is important that epoxy filled cavities are as few as possible because some epoxy types are strongly luminescent.

Several hundred SEM-CL pictures were investigated.. The results included here characterize textures and relations that are general for all the investigated samples.

After different quartz types were recognized by greyscale SEM-CL. Some good quality CL-spectra were achieved at the Department of Geology, University of Oslo, using a Mono-CL. Intensity was adjusted to a certain amount of cps (8000-9000) so the total intensity of the spectra can not be correlated with the trace element content. The relative intensity of the peaks does however give important additional information on the defect structure of the quartz.

4.3 LA-ICP-MS

The analyses of quartz were accomplished with a standard, double focusing sector field, ICP-MS (Finnigan MAT, ELEMENT1) instrument with a CD-1 option from Finnigan MAT and with an UV-laser from Finnigan MAT/Spectrum, Berlin, Germany.

The following elements are included in the analytical package: Al, B, Ba, Be, Cr, Fe, Ge, K, Li, Mg, Mn, Na, P, Pb, Rb, Sr, Th, Ti, U. Where ^{7}Li, ^{9}Be, ^{11}B, ^{27}Al, ^{55}Mn, ^{74}Ge, ^{85}Rb, ^{88}Sr, ^{137}Ba, ^{208}Pb, ^{232}Th, and ^{238}U were analysed at low resolution ($m/\Delta m=300$); ^{23}Na, ^{31}P, ^{25}Mg, ^{47}Ti, ^{52}Cr, and ^{56}Fe at medium resolution ($m/\Delta m\approx3500$) and ^{39}K at high resolution ($m/\Delta m>8000$). The isotope, ^{29}Si, was used as internal standard at low resolution and ^{30}Si was used at medium and high resolution. External calibration was done by using the international standards: NIST612, NIST614, NIST616, BCS313/1(BAS), RGM-1(USGS), SRM1830, Blank SiO_2 and BAM no.1 SiO_2 (Federal Institute for Material Research and Testing, Berlin, Germany). Blank SiO_2 was used to constrain the detection limits (LOD). LOD for most of the elements are between 0.2 and 0.01 ppm. To improve the lower limit of quantification and the analytical uncertainty at low concentrations, it is important to have calibration curves with well-defined intercepts. Laser ablation was accomplished in raster measuring 200x200 μm or less on 200 μm thick quartz wafers. Detailed information about the analytical conditions, recalculation and statistical treatment of the data is described elsewhere (Flem et al., 2002).

The selection of sampling spots in quartzite quartz is complicated by the high density of inclusions, such as muscovite, rutile needles, silimanite, biotite tourmaline and dumortierite. This fact complicated the analysis and many samples could not be ablated although, in the end, an appropriate number of representative quartz types were sampled.

5 Results

5.1 Field observations and Sampling

5.1.1 Quartzites

Fieldwork was done in the Arendal area, South Norway. Sampling was based on five different quartzite textures that were defined in the field::1.*High grade static*: 2.,*High*

grade mylonitic gneisses, 3.*Greyish quartzites,* 4.*Quartz muscovite veins,* 5.*Micro-faults (*Table 1 *below)*

Table 1: Classification of quartz textures observed in the field

Type	Quartzite texture	Description
1	*High grade static*	Blue coarse-grained quartzite. Weakly foliated, Biotite SPO weak to absent, banding between dusty blue/whitish/purple quartz. The associated mineralogy typically comprise Quartz ± Bt± Kfs± Mt± Ilm/Hem and fibrolitic silimanite.
2	*High grade mylonitic gneisses*	Mm-sized amoeboid quartz grains, including grains of biotite ± Tourmaline, which define a continuous foliation
3	*Greyish quartzites*	*Greyish quartzites* with static textures
4	*Quartz muscovite veins*	Veins consisting of quartz and muscovite cutting through textures 1 and 2.
5	*Micro-faults*	separated by zones not affected by the retrogression and with blue type 1 quartzite lenses, crosscutting all other features except for late brittle cracks

Some of the quartzites appear pure and massive whereas more impure quartzites, show banding and lenticular structures. The mineralogy of the quartzites inconsistently varies between K-feldspar-rich and biotite-rich parts. The content of other minerals than quartz also varies considerably. In effect more pure quartzites are coarser grained than impure varieties. In some places the quartzites feature a distinctively banded appearance, with cleavage domains rich in fibrolite and with white mica defining a disjunctive cleavage intersecting microlithons of quartz and biotite (Figure 2). The number of micro faults is generally higher in the cleavage domains. However, the gradual transition between lensoid bodies rich in fibrolite and white mica in the quartzite matrix and banded quartzite with increasing strain, document that these bands probably originate from pre-existing chemical variations (Figure 2). The lensoid shape is usually completely obliterated (i.e. sheared out) in XZ sections (sections cut parallel to the lineation and perpendicular to the foliation), but subparallel to oblique in YZ sections (sections cut perpendicular to lineation and foliation)(Figure 2). In most samples they are oriented parallel with the foliation, but occasionally they are inclined to the foliation at a small angle (Figure 2).

The quartzites along the Frolands Verk road profile (locality 1 see Figure 1) are generally very coarse-grained, and have a bluish tint. Their purity varies significantly on m-scale between 99% quartz and 79-80% quartz. The main structural feature is narrow (mm-cm thick) cataclastic bands locally featuring a greenish colour probably caused by micas. The mineral assemblage of the quartzites comprises variable amounts of microcline, biotite, and muscovite. Biotite is normally present, either fresh or

decomposed to a reddish alteration product or to muscovite. High–grade shear zones are common and in some cases may have a mineral assemblage comprising tourmaline and biotite.

Both static and dynamic high grade fabrics are cut by narrow faults predominantly cataclastic fault zones, with only limited dynamic recrystallisation of quartz.

The quartzites at Ovelands heia (locality 2 see figure 1) are generally more impure than the quartzites from locality 1. In fact the term quartzites only partially apply because the quartz content is usually to low (70-95%). The microcline content is considerably lower than at locality 1, whereas the biotite concentration is much higher. Accordingly the name quartz-biotite gneiss is preferred throughout this study The quartz.-biotite gneisses frequently have a banded appearance at locality 2 and more nodular textures are also found, gradually being sheared into bands (Figure 2). Both bands and nodules are biotite free but rich in muscovite, and fibrolitic silimanite. More quartz rich parts are coarser grained and more bluish. On fresh surfaces local variations between bluish and more greyish quartz are observed (Figure 2). As with locality 1, there is a close relationship between an increase in grain size and purity of the quartzites.

At locality 2, centimetre- to metre scale en echelon quartz veins (see Figure 1) are surrounded by reaction zones of tourmaline, biotite and green muscovite (Figure 3). Gradual transitions from biotite tourmaline to muscovite tourmaline assemblages in the field and atoll textures of biotite within new muscovite grains document that the muscovite formed later at the expense of the biotite (Figure 3). Muscovite bearing quartz veins are also common and may be clearly distinguished from the former type. They occur at a much smaller scale (mm- to cm with) and form finger like structures.

At locality 2, the different quartz types are more easily distinguished when compared to locality 1. The quartz biotite gneisses are darker and have a banded appearance, but in a few places transitions between nodular textures and banded quart biotite gneisses are observed (Figure 2). Nodules and bands are light coloured and consist of muscovite, silimanite quartz and accessory zircons.

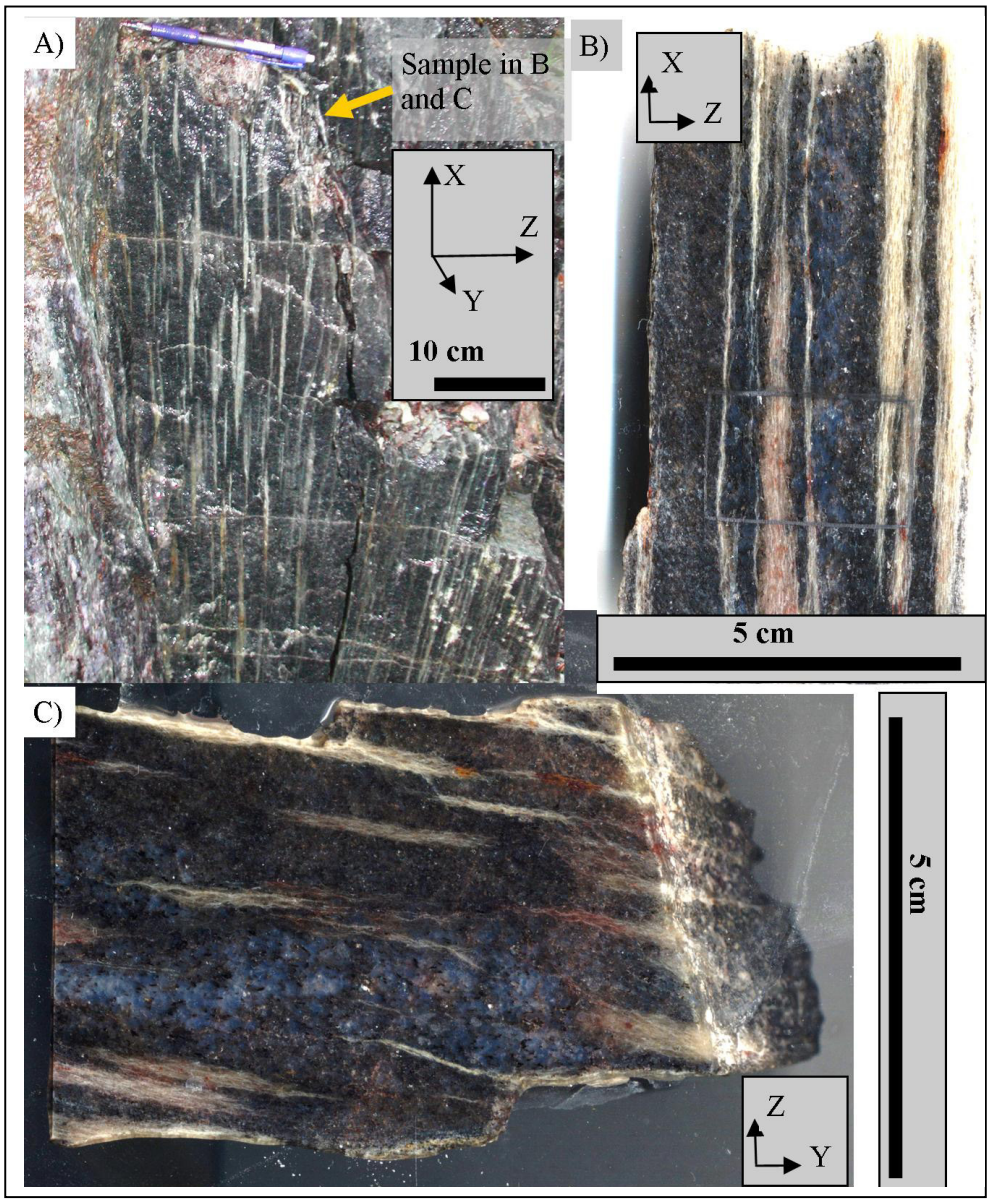

Figure 2: Transition from lenticular/lensoid light coloured bodies to banded quartz mica gneiss from locality 2. A) Field outcrop. Note the gradual change from lenticular structures to the left to bands to the right. B) XZ section showing elongated lensoid structures, traces of the lensoid structures mostly parallel to foliation in sections of this orientation. C) ZY section showing the obliqueness of the lensoid structures with respect to the foliation (horizontal in picture). Note that the light coloured bands are present in both the greyish and the more bluish part of the quartz mica gneiss

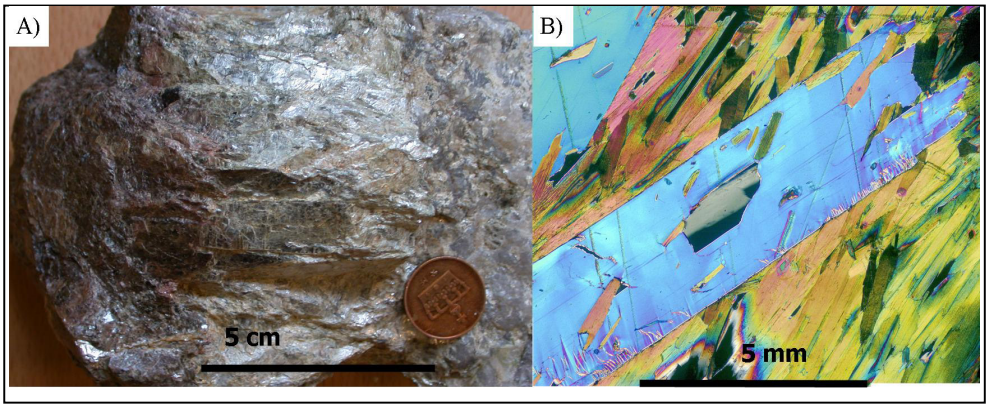

Figure 3: Alteration of biotite tourmaline reaction zone in quartz-mica gneiss at locality 2. A) Hand specimen displaying brown zone of biotite and tourmaline, altered to muscovite and tourmaline in the middle, closest to the contact with the quartz-mica gneiss (rightmost part of picture). B) Thin section image, polarized light, showing muscovite (blue) replacing biotite (greenish to pink). Note the Athol texture with biotite grains engulfed in a large grain of muscovite.

5.1.2 Quartz in amphibolite

Remembering the quartz evolution observed in quartzites encouraged a comparative study of quartz veins associated with the alteration of amphibolite. This was done in order to establish the chronology and relationship of the quartz alteration relative to regional metamorphic and metasomatic events. Quartz veins related to peak metamorphic conditions as well as quartz veins related to retrograde alteration were studied.

5.1.2.1 Quartz occurrences related to prograde metamorphism

Rose quartz veins and garnet quartz symplectites are common in amphibolites but are particularly well preserved at the Skytebanen locality (locality 3).

The rose quartz veins featuring shades of pink, violet and blue, are exposed in amphibolitised gabbro (Figure 8). They are in equilibrium with the prograde metamorphic assemblage in the amphibolites, including almandine rich garnet, tschermakitic hornblende and An_{30} plagioclase and ilmenite.

The garnet quartz symplectites occur in layers mostly comprising quartz, garnet and plagioclase intersecting the garnet amphibolite (see paper 3, Sørensen et al., 2007). Layers are boudinaged with pinches of plagioclase and quartz and swells of mainly garnet and bluish quartz.

5.1.2.2 Amphibolite alteration

En echelon quartz veins with reaction rims of biotite, black tourmaline apatite and actinolitic hornblende are commonly observed in amphibolite, but are especially well exposed at a road outcrop in Osedalen (locality 4).

At Heståsen (locality 5) the alteration phenomena in the amphibolites are particularly well displayed in relation to quartz veins. Three main types of amphibolite alteration were observed: *1. Potassic alteration with biotite introduced in the amphibolites, 2. Potassic alteration with K-feldspar replacing biotite, 3. Massive scapolitisation* (Table 2). For more details on amphibolite alteration see paper 3 (Sørensen et al (2007).

Table 2: Alteration types in amphibolite. From Sørensen and Larsen (2007, paper 2)

Alt1: Potassic alteration with biotite stable
Alt1a: Alteration of amphiboles associated with introduction of biotite. Amphibole cores are dark brownish green whereas rims vary from dark bluish green (Amp3a) through light green (Amp3) to almost colour less (Amp4). **Alt1b:** Veins with a central assemblage comprising plagioclase, calcite, apatite, pyrrhotite, ilmenite/rutile and magnesiohornblende (Amp3). Surrounded by two successive alteration zones, the inner zone comprising amphibole, plagioclase and rutile/ilmenite and the outer zone comprising biotite, plagioclase and ilmenite/rutile. **Alt1c:** En-echelon quartz veins intersecting the foliation in the amphibolite, which comprises both biotite, amphibole and plagioclase Biotite-amphibole plagioclase-ilmenite-(pyrrhotite) bearing reaction zones around en echelon quartz veins **Alt1d:** biotite amphibole rock. Titanite most common, but ilmenite preserved as cores together with rutile. Similar to the alteration around the en-echelon quartz veins
Alt2: Potassic alteration K-feldspar replacing plagioclase e and biotite
Replacement of biotite by K-feldspar. final alteration product is a light grey rock consisting of K-feldspar, and light green amphibole (amp4). Titanite is very abundant in this rock type and almost no ilmenite/rutile is observed. Several types of replacements are seen replacing Alt1 assemblages
Alt3: scapolitisation
Massive scapolitisation. Quartz veins surrounded by reaction rim of scapolite, but minor amounts of scapolite are also observed in many places in the amphibolite. The Quartz vein with the reaction rim of scapolite has a different colouration than the quartz vein with less scapolite. The scapolite has a white colour and is only distinguished from commonly occurring white feldspars by its pronounced cleavage

5.2 SEM-CL/optical textures

Generally, four types of optical textures are observed in the quartzites. The coarse-grained quartzites with blue quartz typically show static textures, with undulose extinction being the only sign of deformation and with randomly oriented biotite. The

high-grade quartzite textures are cut by high grade mylonitic gneisses with grain sizes of several mm's. These are again cut by lower grade cataclastic deformation and occasionally subgrain rotation (SGR)-related deformation microstructures. The SGR relates to the formation of white mica and the breakdown of Biotite to Muscovite (Figure 5 and 6). Chess board textures are commonly observed in the more coarse-grained quartz, but are especially clear and well preserved in quartz veins in the amphibolites (Figure 10).

Four main types of quartz are defined by SEM-CL textures: Qz1: island channel texture, Qz2: light grey, Qz3 diffuse dark grey channels and Qz4: Narrow cracks and pods of non luminescent quartz (see Table 3 below and Figure 4).

Table 3: Quartz types defined by textures in SEM-CL images

Quartz type	Description
Qz1	Bright islands surrounded by darker cracks. Typically partially luminescence quenched.
Qz2	Light grey, sometimes with weak oscillatory zoning. Brighter cores and darker rims, approaching the luminescence of type 3.
Qz3	Dark grey diffuse fluid channel texture, which follows grain boundaries or cut through grains.
Qtz4	Narrow cracks and pods of black quartz, crosscutting the other types.

Fluid inclusions related to quartz types Qz1, Qz2 and Qz3 are absent in the quartzites, but occur in quartz veins in the amphibolites. These fluid inclusions were studied by Sørensen and Larsen (paper 2, 2007) who defined a fluid evolution from CO_2 rich fluids (Qz1) through coexisting low salinity CO2-rich H2O-CO2 fluids and eutectic salinity CO_2-H_2O-NaCl-KCl brines (Qz2) towards NaCl-$CaCl_2$-H_2O brines (Qz3) and ending with $CaCl_2$-H_2O fluids (Calcite).

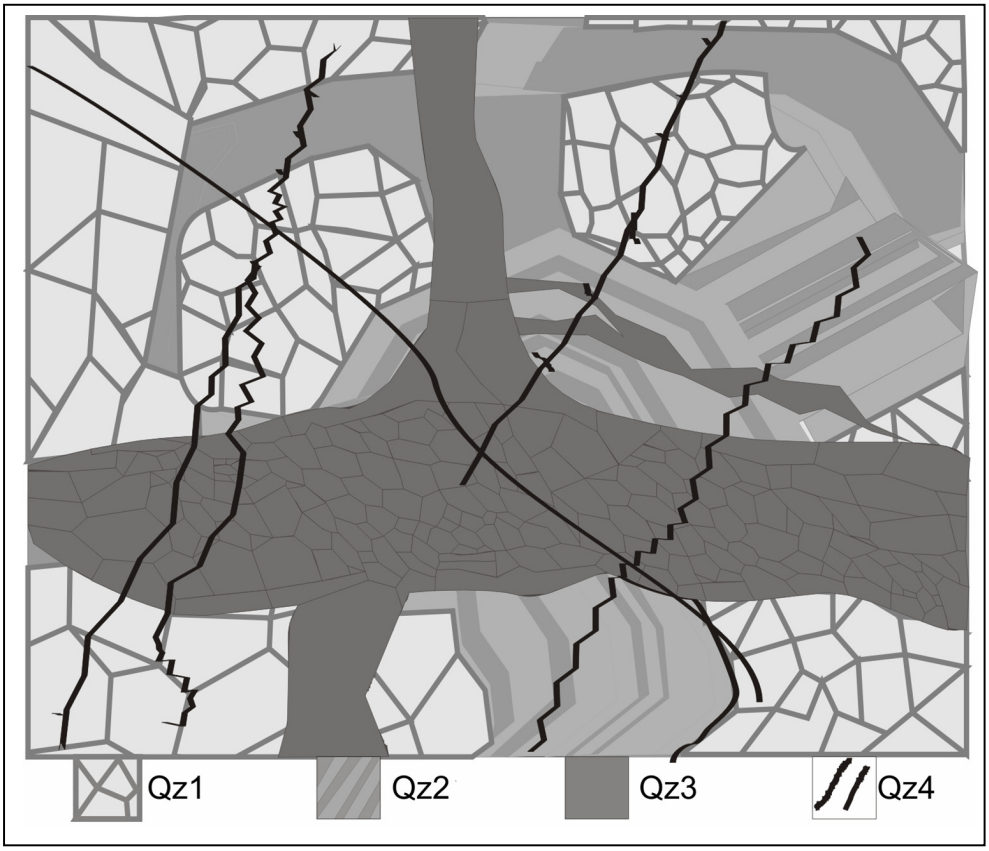

Figure 4: Schematic representation of the quartz textures observed in this study. See text and Table 3 for explanation.

5.2.1 Textural relations in quartzites

Generally there is a good correlation between the naked eye optical textures and the quartz evolution observed in the SEM-CL images. The coarse-grained bluish quartzites mainly consist of Qz1, whereas Qz2 dominates in the more greyish quartzites and in some mylonitic gneiss. Qz3 is the most rare quartz type and is typically related to localized SGR textures and alteration of biotite to muscovite,

Sample 03bes32 (Figure 5) demonstrates the relation between the quartz types and the transition from bluish quartzite to greyish quartzite (Figure 5). The more bluish part of the section is very coarse-grained. In the SEM-CL this corresponds to a mixture of (Qz1) and (Qz2). Of theses types, Qz2 dominate, followed by Qz1. Qz2-Qz2 grain boundaries are commonly straight with triple junctions, whereas Qz1-Qz2 grain boundaries are interlobate-lobate, with pinning, window, dragging and “left over grain”

microstructures (see e.g. Passchier and Trouw, 2005 for definition) implying the growth of Qz2 at the expense of Qz1 (Figure 5)

A distinct luminescence quenching (Qz3) affecting both Qz1 and Qz2 occur where biotite grains are partly altered to muscovite, and inside quartz grains in channel like structures connecting muscovite grains (Figure 5). Biotite flanking these channels is partially or completely altered to poikiloblastic muscovite (Figure 5). Qz3 is also common next to sub-millimetre thin fault zones, where a smaller grain size is developed in Qz3 only. Qz1 is partially luminescence quenched, and based on luminescence, may be difficult to distinguish from Qz2. Preferably Qz1 and Qz2 are differentiated by recognition of the island channel texture. Notably the intensity of the CL-signal increase in Qz1 next to more deformed areas (Figure 5).

Alteration of ilmenite grains to rutile is seen in more coarse parts of the sample. The proportion of rutile formed at the expense of ilmenite correlates with the amount of Qz2 present (Figure 5). Locally weak SGR textures are observed, always in association with Qz3 (Figure 5).

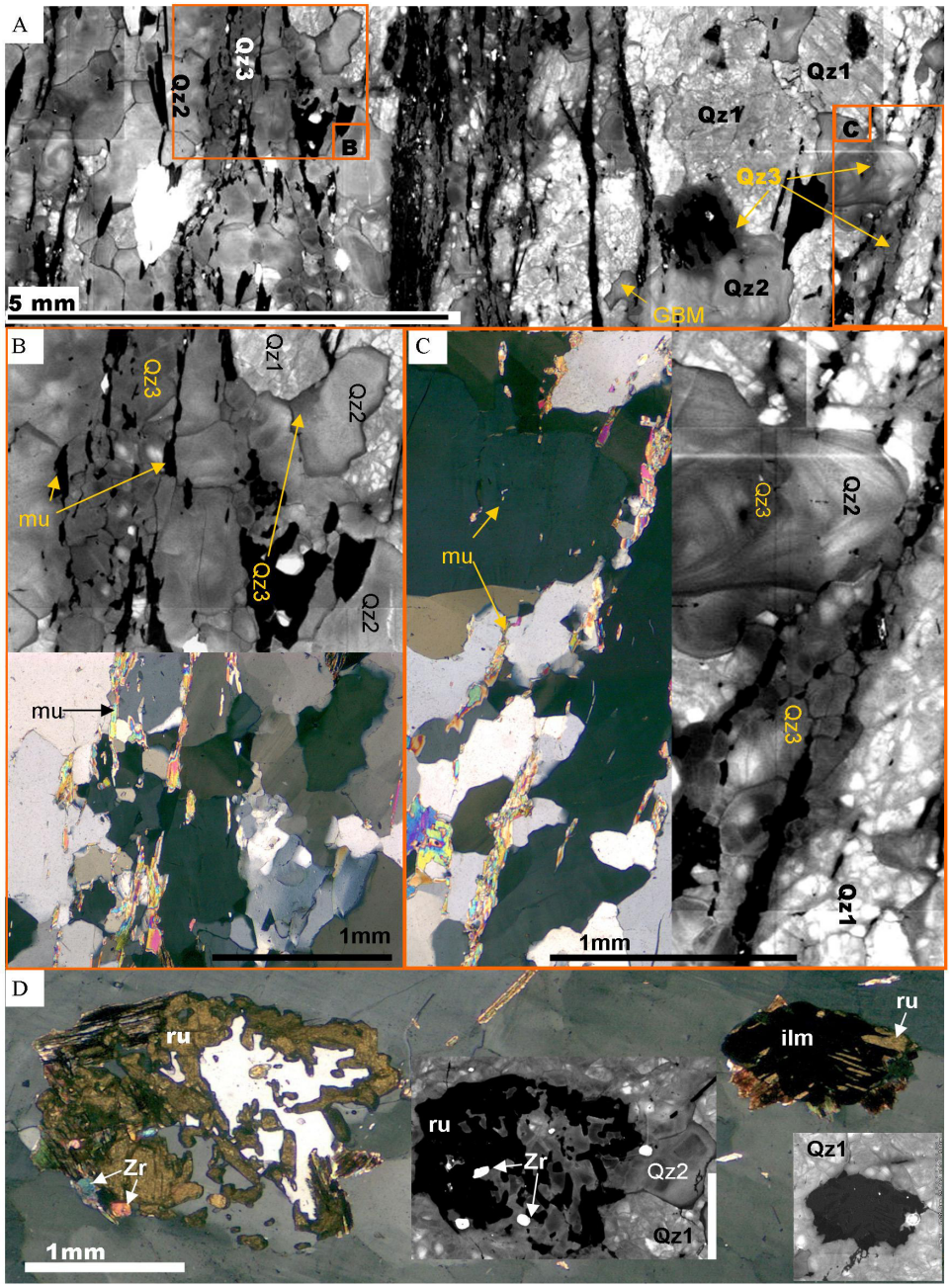

Figure 5: Optical and SEM-CL textures from 03bes32. a) Large scale SEM-Cl textures from part of 03bes32, showing relation between Qz1, Qz2 and Qz3. Note that the main proportion is Qz2. Note that Qz3 transects both types Qz1 and Qz2. b) Zoom on (a) and optical picture of the same area. Note the spatial relationship to white mica, and grain

size reduction of quartz in areas with Qz3 C) Zoom on (a).Qz3 cuts oscillatory zoning in Qz2 and relate to grain size reduction and formation of white mica D) Ilmenite partly altered to rutile, most altered grain related to Qz2, whereas well preserved relates to Qz1

In sample 03bes71, also from locality 1, the relations between Qz3 and deformation are better seen than in 03bes32, because the amount of Qz3 is larger. The sample was gathered at the transition from coarse-grained bluish quartzite to pale quartzite with numerous narrow micro-faults (Figure 6). In the hand specimen, lenses of more bluish quartz occurs in strongly deformed and bleached domains (Figure 6). These domains are also recognized in optical and SEM-CL microscopy (Figure 6). Optically they are more coarse-grained and biotite is well preserved with only local alteration to muscovite. In the SEM-CL pictures it is evident that the coarse-grained lenses comprise Qz1 and Qz2. Places in the coarse-grained domains, where biotite is partly altered to muscovite are connected with luminescence quenching of Qz2 towards Qz3. Accordingly, both quartz types Qz1 and Qz2 coexist with biotite. Adjacent to the coarse-grained domains, the quartzites are more deformed in both cataclastic and plastic structures accompanied by dynamic recrystallisation dominated by SGR causing a reduction of the grain size to less than 200 microns and the formation of more polygonal grains, defining an oblique fabric, documenting a sinistral shear sense (Figure 6). This corresponds to relative upward movement of the SW block relative to the NE block in the direction of the oblique lineation observed in the field areas with SGR restricted to Qz3. Deformation related to SGR textures continues as narrow cataclasite bands when entering other quartz types or disappear (Figure 6), suggesting different responses to deformation as a function of quartz types. The SEM-CL intensity of Qz1 increase towards zones where Qz3 is deformed by SGR compared to Qz1 in the less deformed areas.

In sample 04bes71 Qz3 is also common in coarse-grained parts of the sample as channel like structures commonly connecting grains of biotite that are partially altered to muscovite (Figure 6). Not only does the channel structures connect partially altered biotite grains, but the luminescence quenching textures also correlates with grain scale alteration textures in the individual biotite grains, such that biotite is exposed toward quartz types Qz1 and Qz2 whereas muscovite appear next to type 3 quartz (Figure 6).

Quartz muscovite veins are commonly observed. They are decussate with muscovite grains in a matrix of Qz3 (Figure 7). The formation of Qz3 in relation to the quartz muscovite veins is featured by sample 03bes103 (Figure 7). Dissolution of Qz1 relates to precipitation of Qz3 together with muscovite in veins fingering their way through the Qz1 and Qz2 matrix. Parallel cracks interpreted as microfaults are seen in a Qz1 grain (Figure 7). The microfaults are connected with luminescence quenching textures that tapers in to the quartz muscovite veins (Figure 7).

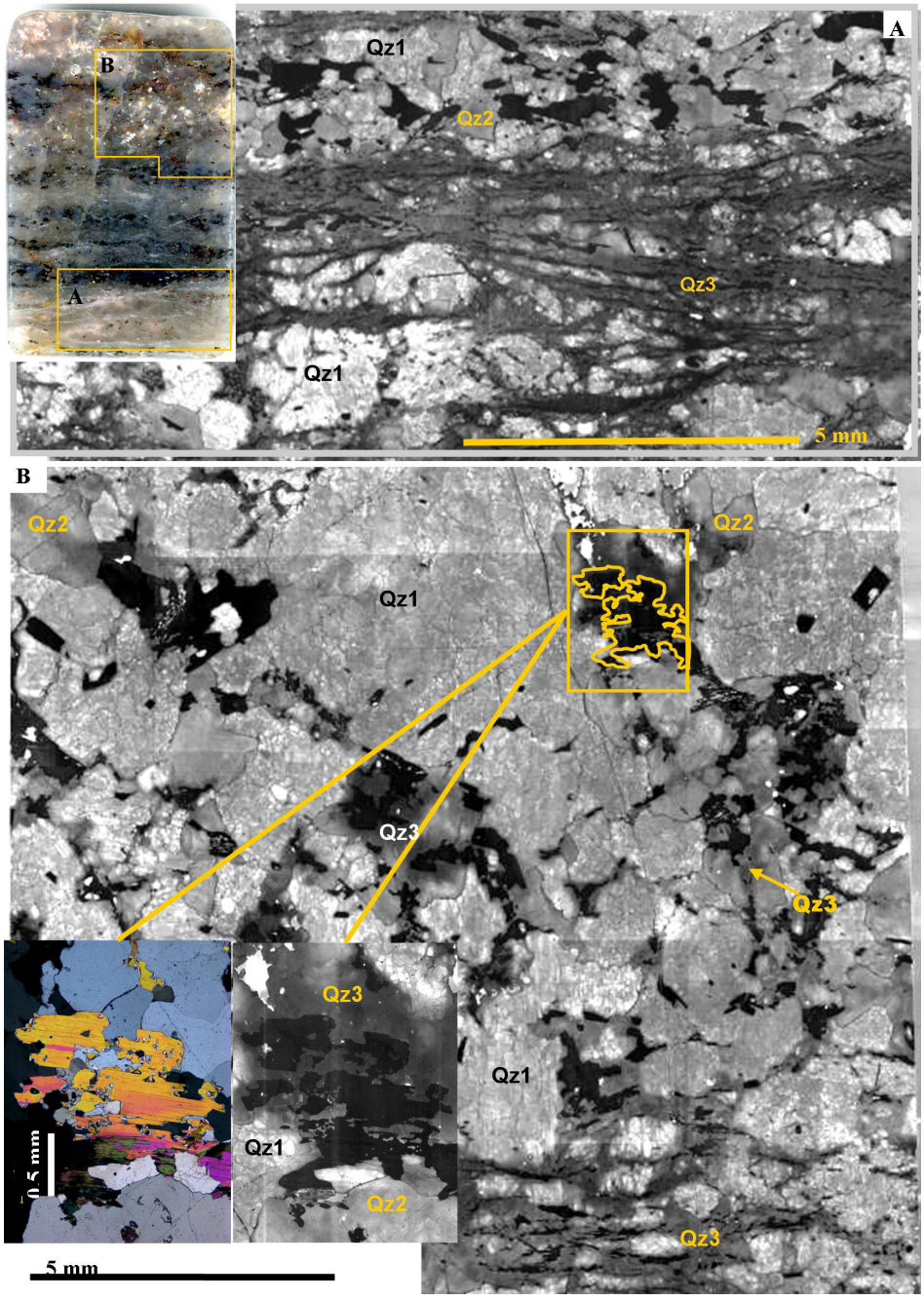

Figure 6: See caption on next page

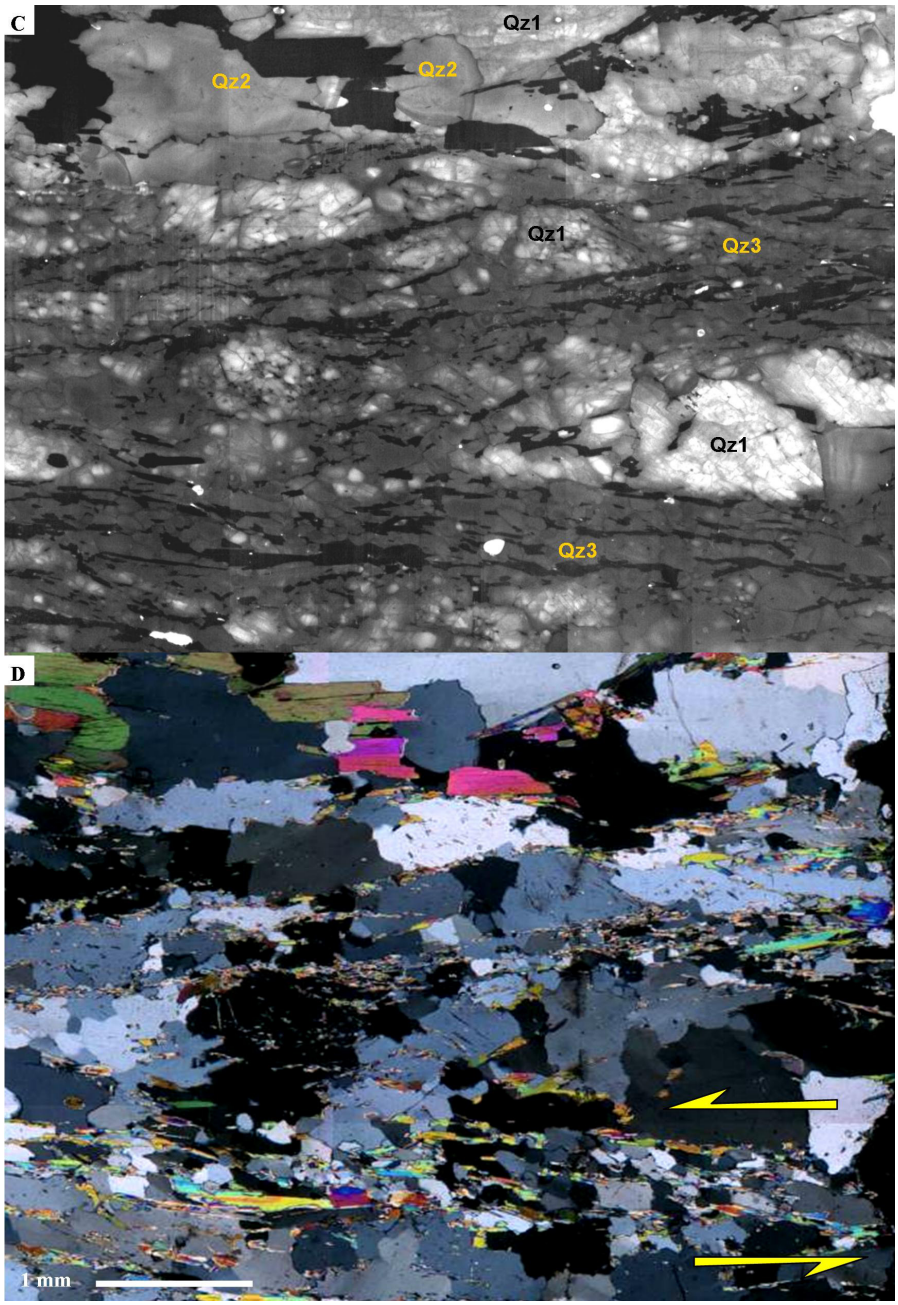

Figure 6: Optical and SEM-CL textures from 03bes71, insert show the position of the large SEM-CL pictures (A &C) on the rock slab. A) Large SEM-CL picture of a deformed zone showing the distribution and textural relations amongst Qz1, Qz2 and Qz3. B) Image from a more coarse-grained part of the sample dominated by luminescence quenched

Qz1, Note however the network of Qz3 connecting mica grains. Zoom on (C) shows the spatial relationship between muscovite (bright interference colours), biotite relics and Qz1-3. Note how biotite relics in the optical picture correlates with Qz1, whereas the pure muscovite part of the grain is exposed against Qz3. C) Zoom on (A), showing the SEM-CL textures D) Optical image of the same region as in (C). Note that SGR optical textures in D between the yellow arrows occur only in connection with Qz3 in the SEM-CL image (C).

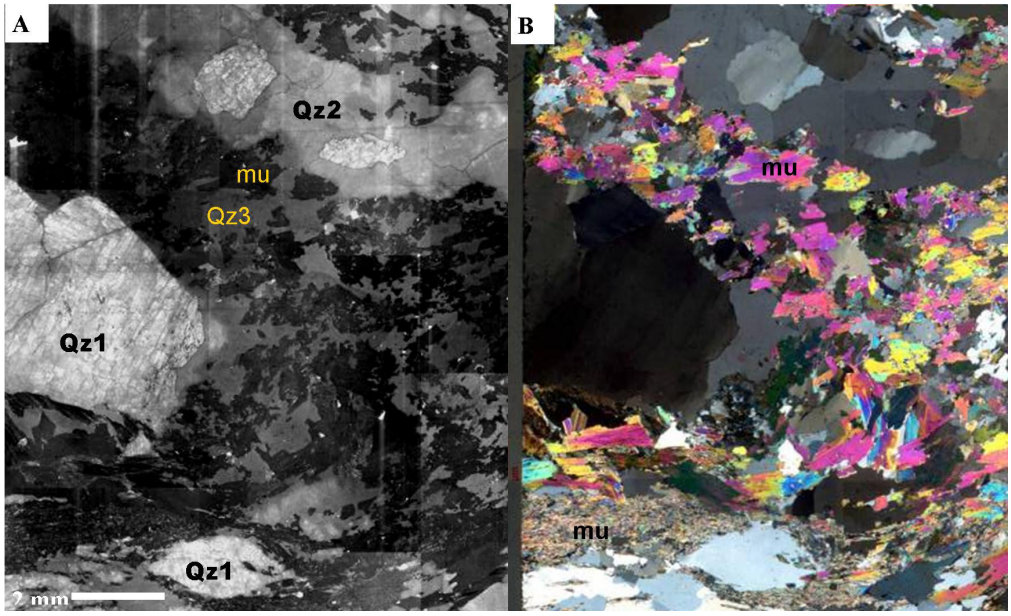

Figure 7: Optical and SEM-CL textures from 03bes103 quartz muscovite veins, showing optical and SEM-CL textures of quartz muscovite vein in quartzite. A) SEM-CL image. B) Optical image. Same area displayed in both images. See text for discussion.

5.2.2 Textural relations in quartz in amphibolite

SEM-CL images rose quartz veins in amphibolite has the highest luminescence of all the studied samples (Figure 8). Rose quartz is characterised by numerous crystallographically orientated needle shaped inclusions. Luminescence quenching is weak and primarily occurs along grain boundaries (Figure 8). The island texture defining Qz1 is also present in this sample, but Qz2 is absent (Figure 8). The cracked grains of Qz1 are intersected by non luminescent quartz in few microns thick trans- and circum granular cracks (Figure 8). The latter quartz type was classified as Qz4 and was not analysed by LA-HR-ICP-MS because the high density of mineral and fluid inclusions would have interfered with the analysis.

Blue quartz similar to bluish quartz in the quartzites occurs in garnet quartz symplectites at the same locality as the rose quartz veins. However, the garnet is more almandine rich, and the amphiboles are more Al-rich and hastingsitic compared with the garnet amphibolite (see paper 3, Sørensen et al., 2007). Ilmenite and chlorapatite is also common in the garnet quartz symplectites. Unidentified prismatic solid inclusions in apatite contain CO_2 fluids at their tips. The texture of quartz in the garnet quartz symplectites consist of bright islands surrounded by cracks with less luminescent quartz (Qz1) (Figure 8). Some Qz2 is also present. Qz1 is brecciated and luminescence of the cracks in Qz1 is the same as in Qzt2 (Figure 8). The brightest and least brecciated Qz1 is preserved as inclusions in garnet in the garnet quartz symplectites or as inclusions in tourmaline in quartz tourmaline leucosomes (Figure 8). The quartz in quartz-garnet leucosomes and in garnet quartz symplectites in other places show similar textures (Figure 8).

En echelon quartz veins at locality 4 are surrounded by a reaction zone comprising green acicular hornblende, biotite, ilmenite, apatite and plagioclase (Figure 9). Plagioclase is partially sausuritised and sericitised (Figure 9). Ilmenite is completely or partly replaced by titanite (Figure 9). The quartz within the quartz vein mostly consists of Qz2 with minor amounts of Qz1 (Figure 9). Both Qz2 and Qz1 are intersected by trans, inter, circum- and intragranular cracks that may only appear in the SEM-CL images as features belonging to Qz4 in sub-micron thick cracks with black CL (figure 9)

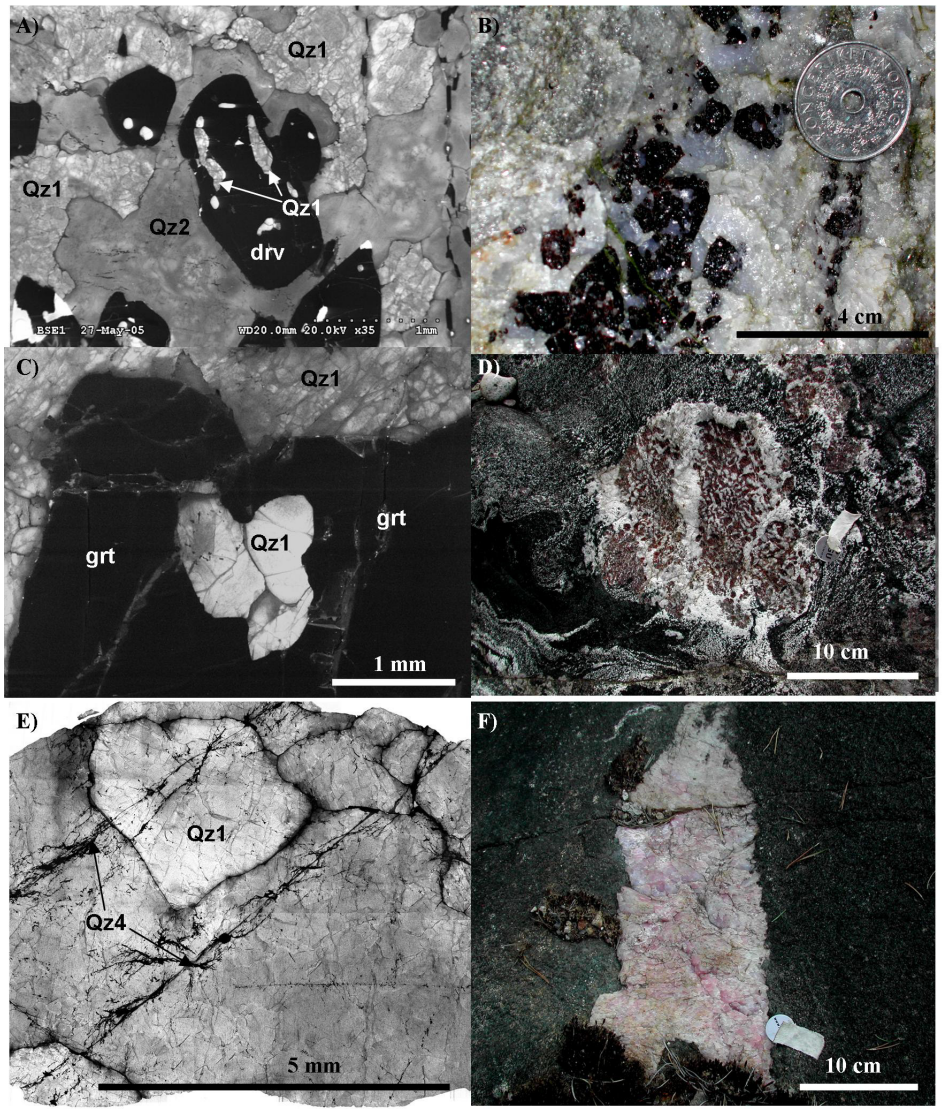

Figure 8: Optical and SEM-CL textures from garnet quartz symplectites, rose quartz veins, garnet bearing quartz leucosomes in amphibolite and intergrowths between quartz and tourmaline in quartz tourmaline gneiss A) SEM-CL image showing Qz1 inclusions in dravitic tourmaline (drv) in a matrix of Qz1 and Qz2 B) Field image showing the co-occurrence in leucosomes of dravitic tourmaline and blue Qz1 C) SEM-CL image showing bright Qz1 inclusions in garnet and more luminescence quenched Qz1 and Qz2 outside garnet D) Field picture of garnet quartz symplectite E) SEM-CL image of rose quartz vein, consisting of Qz1, cut by trans– and circumgranular cracks of Qz4 F) Field image of rose quartz vein in garnet amphibolite.

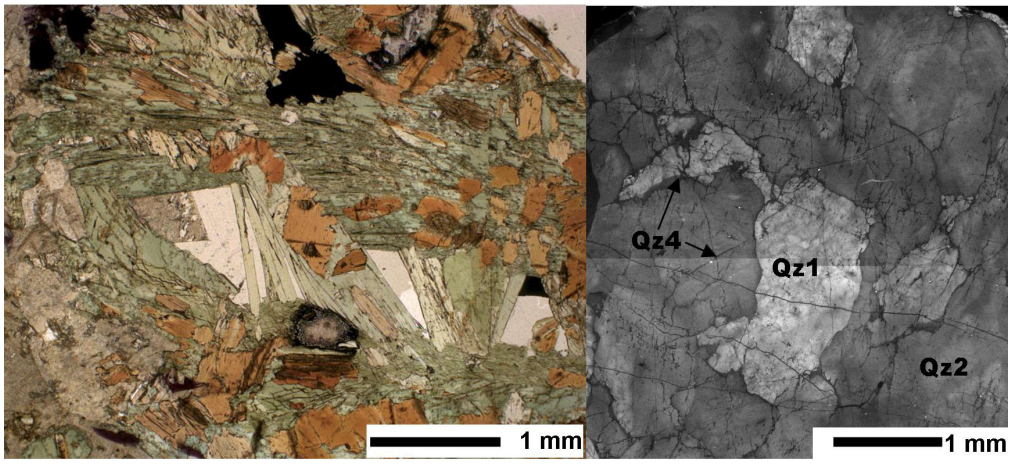

Figure 9: En-echelon quartz vein from locality 4. A) Decussate biotite-magnesiohornblende in a reaction texture enveloping the quartz vein. B) SEM-Cl image showing Qz1 and Qz2, both intersected by cracks with Qz4. See text for explanation

Quartz veins in amphibolites having the different alteration stages in locality 5 described in Table 2 (p.10) were also investigated by SEM-CL:

Quartz veins surrounded by alteration type 1 comprising greenish black amphibole (field colour) and biotite mainly consist of Qz1 and Qz2. Samples 04bes143, 04bes120 and 04bes121 are examples of such veins. They only contain minor amount of Qz3 (Figure 10). Qz2 in these samples is coarse-grained (Figure 10) and features a high density of coarse rutile. Qz1 also contain many needle shaped inclusions, but they are much finer. The optical microstructures of Qz1 and Qz2 are different; Qz1 comprises a chessboard texture of subgrains, whereas Qz2 has more even extinction pattern although it often display deformation lamellae (Figure 10). The chessboard microstructure is partly overprinted by basal subgrain microstructures, which relate to an increase in the luminescence intensity (Figure 10).

Quartz veins in alteration type 1 with lighter shades of green amphibole and lighter coloured biotite and alteration type 2 mostly consist of Qz1 and Qz2 (Figure 11), but both Qz1 and Qz2 have significantly lower luminescence intensity, when compared to quartz vein in alteration type 1 with darker amphibole and biotite (see Table 2 for definition). Qz3 is not very abundant in quartz veins in alteration types 2 and 3 but occurs as a diffuse channel system, altering the other quartz types (Figure 11).

The quartz-scapolite veins (Alt3) also consist of more than one quartz type (Figure 12), but the overall intensity is much lower than in the other samples, hence most of the quartz is classified as Qz3. However, some of the Qz3 appears homogeneous both in optical and SEM-Cl pictures, where subgrains are seen in both SEM-CL and optical images on the more luminescent Qz3 (Figure 12). Both Qz3 subtypes are intersected by micron thick irregular cracks of Qz4, which correlate with numerous solid inclusions of calcite and calcite bearing fluid inclusions (figure 12).

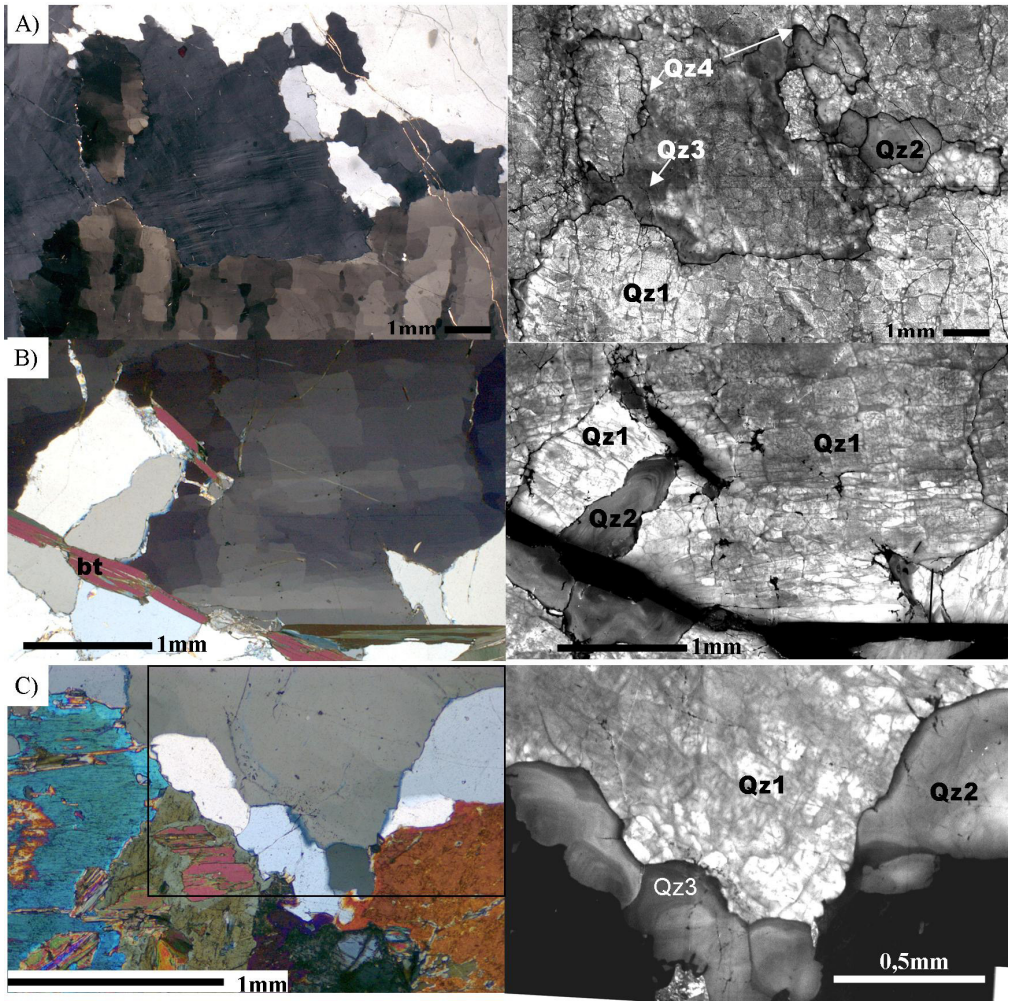

Figure 10: Comparison of optical and SEM-CL textures in quartz veins in amphibolite with alteration type 1 (see text). A) 04bes121, the least altered sample, consisting of Qz1. Note the chessboard pattern in the optical microstructure coinciding with the island/channel texture (Qz1) in the SEM-CL image. Note also the deformation lamellae in the central luminescence quenched grain, consisting of both Qz1 and Qz2 and that the luminescence quenched grain consume the brighter grain (upper right). Note also that there are grain boundary textures at different scales; grain boundaries are lobate with Qz2 overgrowths consuming Qz1 but grains boundaries are also serrated at a finer scale with very dark to non luminescent quartz overgrowths consuming all other quartz types. B) 04bes120, mostly consisting of Qz1 with minor amounts of Qz2 and Qz3. Note chess board texture overprinted by elongated prismatic subgrains. In the lower part of the middle Qz1 grain, the prismatic subgrains override signs of the chess board texture, which is more pronounced in the upper part of the grain. In the corresponding SEM-CL

this shift in the microstructure is also detected. Note that the luminescence increase as the prismatic subgrains become more pronounced. C) 04bes120 polarised light micro photo showing the connection between amphibole alteration related to the introduction of biotite and formation of Qz2 in the lower part of the SEM-CL picture. Note also the dark grey Qz3 overgrowths on the Qz2 grains.

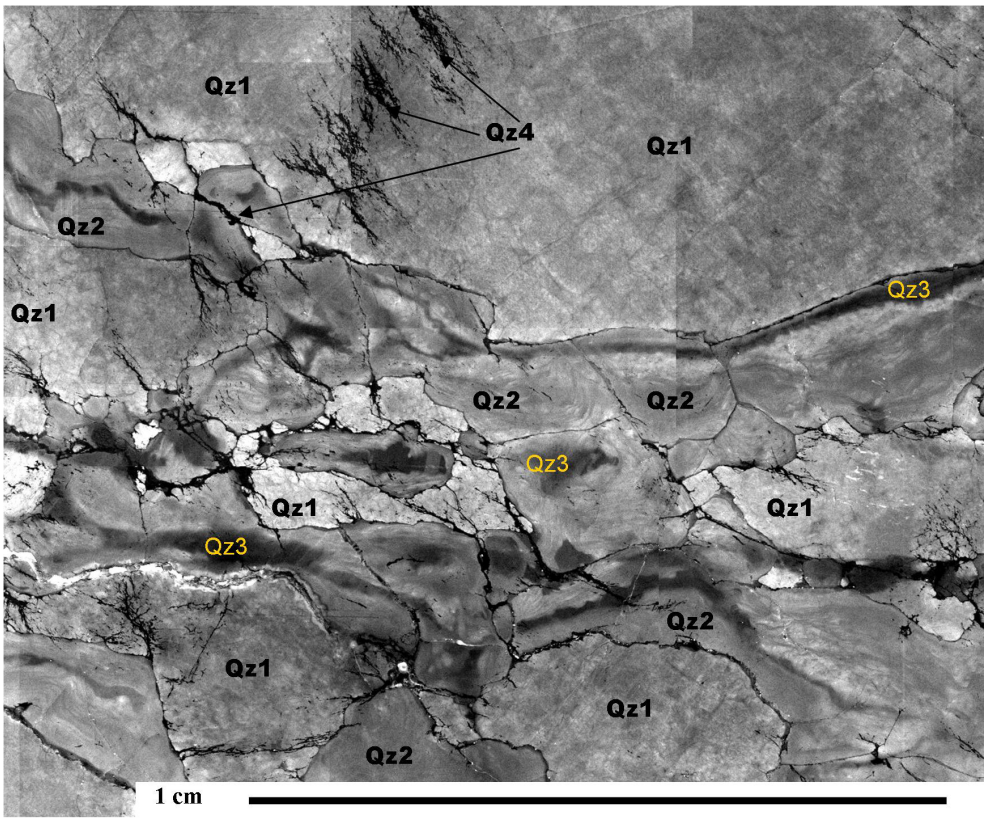

Figure 11: Optical and SEM-CL textures in quartz vein (04bes91), surrounded by alteration type Alt1 with bleached actinolite and light brown biotite (se text and Table 2). Note that the contrast setting in the SEM was increased, compared to the other samples in this paper to see the textures in this sample, which generally are low luminescent. The difference between Qz1 and Qz2 is hardly recognised in this image, but may be differentiated by the barely recognisable cracked texture of Qz1 and the faint oscillatory zoning in Qz2. Qz3 in this sample display a partly connected channel network. Qz4 is also seen as cracks in the large Qz1 grain to the right.

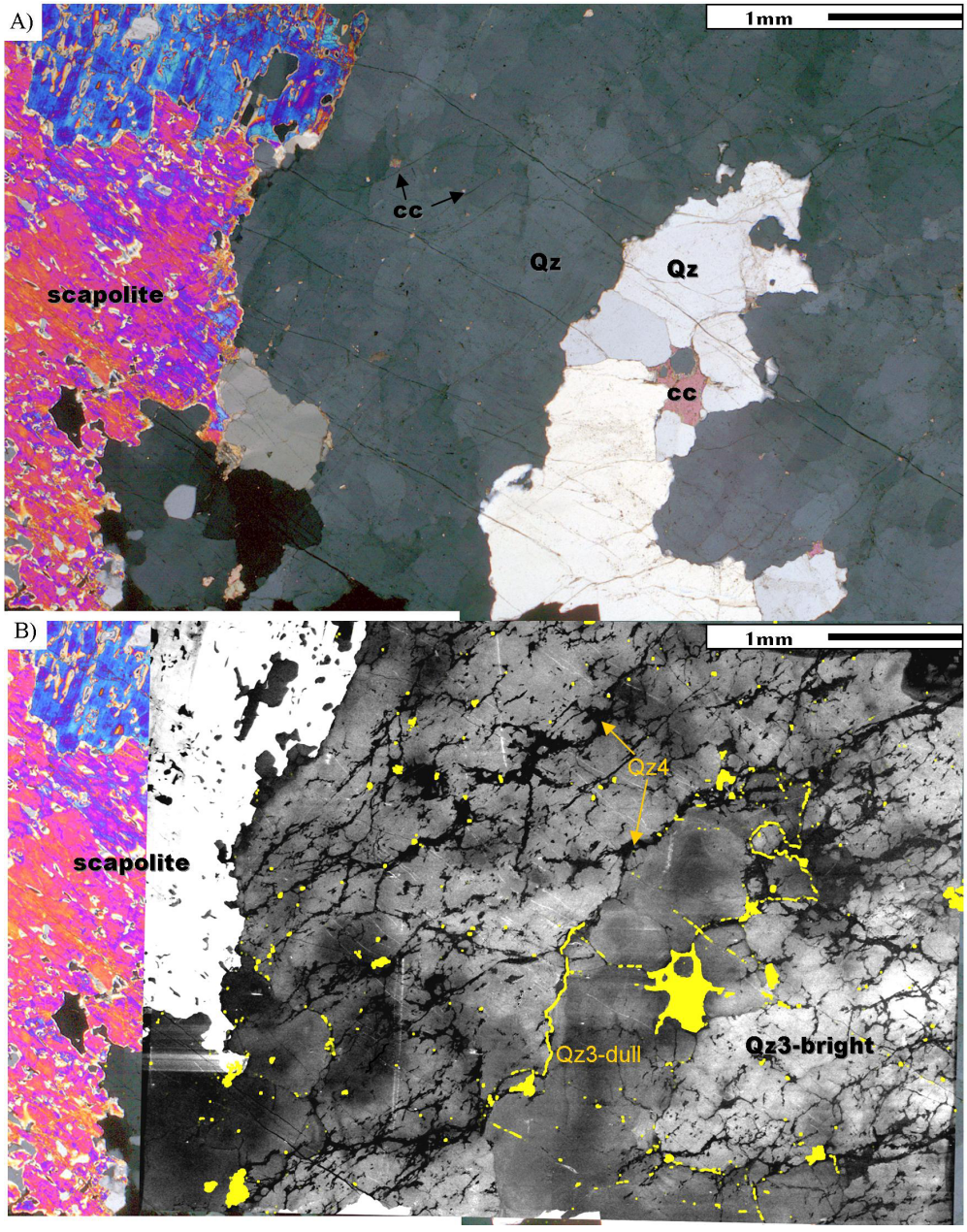

Figure 12: Optical and SEM-CL textures in quartz scapolite vein (04bes122, Alt3). A) Optical picture, showing scapolite to the left of the quartz vein consisting of two quartz types. One quartz types has a distinct subgrain texture whereas the other quartz has a more even optical extinction pattern. Note the many bright luminescent calcite inclusions in the quartz matrix. A larger calcite inclusion is seen in the middle bright quartz grain.

B) SEM-CL of the same area as in (A). Note that the contrast setting in the SEM was increased, compared to the other samples in this paper in order to image the textures in this sample which generally is low luminescent. The quartz with subgrains is higher and more unevenly luminescent than quartz with the even optical extinction pattern. Note luminescence quenching next to the Scapolite. Both the light grey and dark grey quartz in this image are classified as Qz3 by comparing with luminescence of other samples. Both light and dark grey Qz3 is cut by irregular trans and circumgranular cracks with Qz4. Yellow patches marking calcite inclusions detected by optical microscopy all correlate with Qz4 cracks

---

5.3 SEM Mono-CL spectra

Some samples were investigated by SEM-Mono-Cl to investigate the defect structures creating the contrast between the different quartz types. The results of the spectral analysis are shown in Figure 13. Because Qz1 had the largest variability in texture (degree of brecciation and luminescence quenching) and chemistry, Qz1 was investigated by SEM-mono-Cl in several samples. In most samples, Qz1 is dominated by at high peak at 350-470 nm, probably related to Ti defects in the quartz lattice and a peak at 500-670 nm probably related to H_2O and intrinsic defects (e.g. Goetze et al., 2001). The 500-670 nm peak is less dominant in bright Qz1. Rose quartz vein has a different spectra from that of the blue quartz with distinct peaks at 370 nm, 420 nm and 440 nm.Qz2 has the same peaks as Qz1, but the 500-670 nm peak is stronger when compared to the 350-470 nm peak. Qz3 only features the 500-670 nm peak indicating that H_2O related defects and intrinsic defects are the only significant defect in this quartz type.

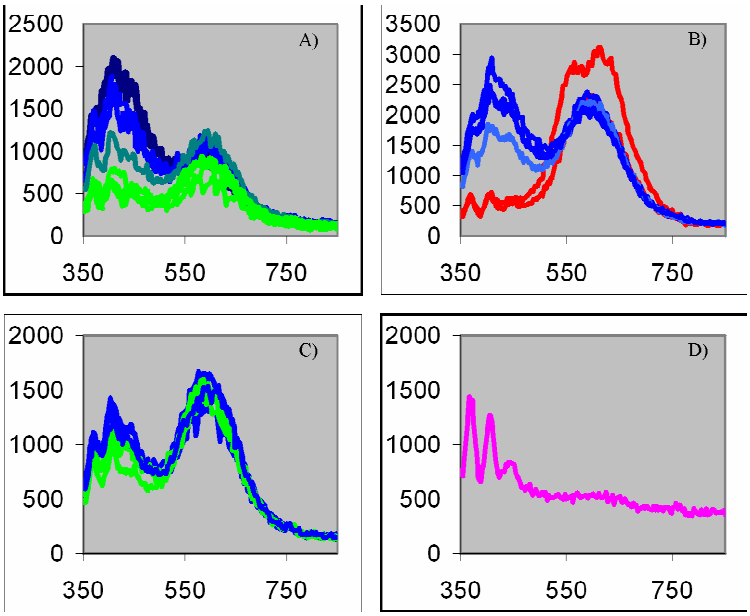

Figure 13: SEM-CL spectra of the studied quartz types, similar scales of wavelength in nm on the horizontal scale. Blue lines are Qz1, green Qz2, red Qz3 and the pink is Qz1 in rose quartz veins. Y-Scale is intensity (cps). A) Qz1 and Qz2 in garnet quartz symplectite, darkest blue represent bright well preserved Qz1 included in garnet,

blue bright Qz1 outside garnet and greenish blue duller Qz1. B) Qz1 same colour scheme as in A. Qz3 red C) Qz2 and dull Qz1 from quartzite (04bes32). D) Bright Qz1 in rose quartz vein (04bes99).

5.4 Quartz chemistry vs. texture

A wide range of trace elements were measured in the three quartz types Qz1, Qz2 and Qz3. Figure 14a show the mean value and standard deviation of each element in the quartz types. Only Ti, Al, K, and P occur in significant amounts (Figure 14a). All other elements are either below detection limits or in sub-ppm concentrations. Ti is the most significant discriminator between the quartz types, both in quartz vein and quartzites (Figure 14a). The average Al content is higher in Qz1 than in the other Qz types, and is also higher in quartz veins in amphibolites than in quartzites (Figure 14a).

A plot of Ti versus Al shows that quartz from the study area represents a wide compositional range (Figure 14b). Qz1 show the widest compositional range and is the only quartz type featuring considerable Al contents. Al in Qz1 varies from 50 to several hundred ppm (Figure 14b). At closer inspection, Qz1 falls in two groups, when B, Ti and Al contents are also considered (Figure 14b). The extremely high Al contents only occur in rose quartz (Figure 14b), whereas garnet quartz symplectites has much lower contents of both B and Al (Figure 14b). There is no systematic variation in the typical Al content between the Qz types (Figure 14e), although Qz1 has larger variation than the other Qz types.

At Ti contents below 100 ppm, the Al content is relatively low and constant, but at higher Ti contents Al increase dramatically (Figure 14b). There is a strong correlation between Al and B especially at High Al concentrations i.e. the linear trend in Figure 14c. This linear trend is followed by Qz1 in amphibolites but not by Qz1 in quartzites (Figure 14c). The inclination of the trend line in Figure 14c matches the B/Al ratio in Dumortierite $(Al_{6.5\text{-}7}(BO_3)(SiO_4)_3(O, OH)_3$. Accordingly the large variations in the Al content in Qz1 in Qz in amphibolite, do not relate to structurally incorporated Al, but rather is the result of micro-inclusions. All Qz types have the same distribution of Al content, with a typical average at 15 ppm (Figure 14e).

Qz2 show considerable variation in the Ti content (from 20-100 ppm) but generally has Al contents below 50 ppm (Figure 14b). This is also reflected in the Boron content which is also low in type 2 quartz as seen in the trend between B and Al for higher Al concentrations (Figure 14b). The variations in the Ti content of Qz2 are much larger for the quartz veins in amphibolite than for Qz2 in quartzite (Figure 14d). A frequency plot suggest that the variation in the Ti content in Qz2 in quartz veins in the amphibolites is random (Figure 14d), whereas the Ti content in Qz2 in quartzites varies systematically around a type value of c. 22 ppm (Figure 14d). Partially this could be the result of rutile needles that vary in density between the samples. However Qz2 also formed during fluctuating conditions as demonstrated by oscillatory zoning and edge ward decreasing luminescence possibly associated with the formation of Qz3 (Figures 5-11). Qz3 sometimes follow the grain boundaries of Qz2 (Figures 5-11). In relation to

darker rims on Qz2 the alteration of biotite to muscovite is common (Figures 5 and 6). Accordingly the dark rims on Qz2 possibly are overgrowths of Qz3.

Apparently, Ti is easily leached from Qz1 whereas Al and B rarely are lower than 50 ppm. Conversely Qz2 and Qz3 consistently show low Al below 50 ppm (Figure 14b). Even in samples where the Qz1 is so luminescence quenched that it is almost indistinguishable from Qz2 and Qz3 still contain significant amounts of Al and B (Figure 14d).

Qz3 has trace element content close to or below the detection limits i.e. it has a very well defined chemical signature (Figure 14a-d). In addition Qz3 feature almost the same chemistry in both amphibolite and quartz veins and in quartz-muscovite veins, except for phosphorous which apparently is higher in the quartz-scapolite veins than in the quartzites (figure 14a).

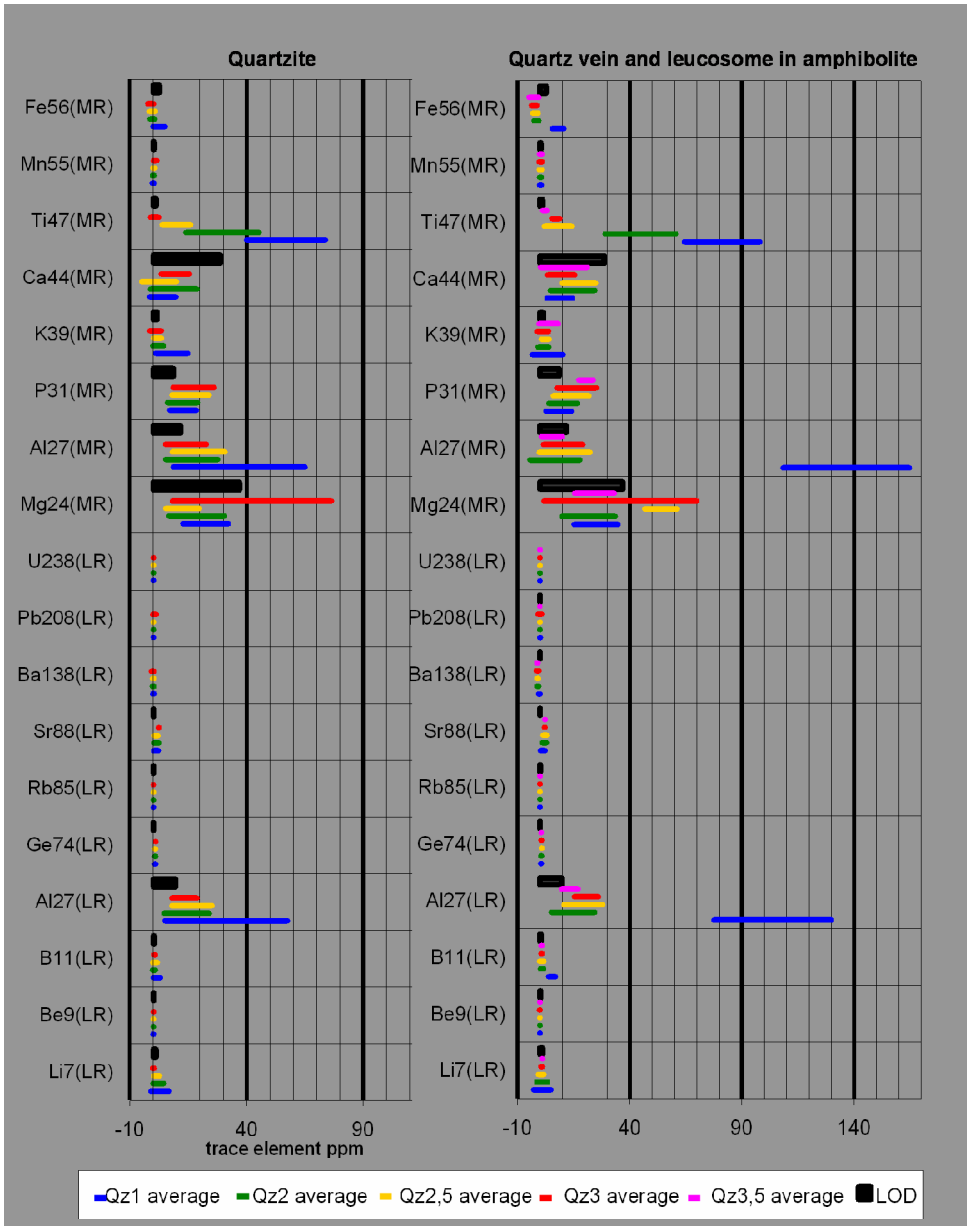

Figure 14: See caption on next page.

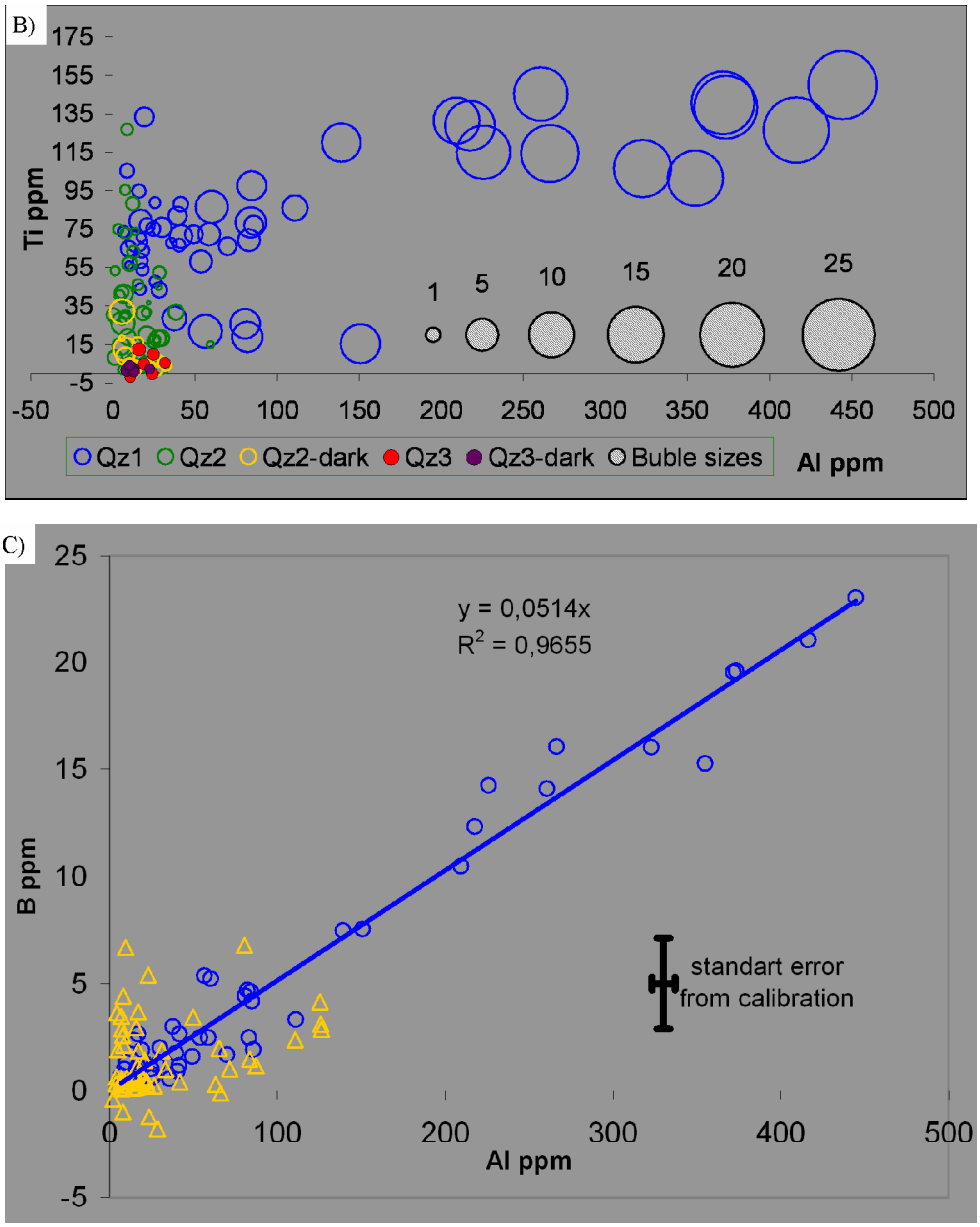

Figure 14 continued. See caption on next page

D)

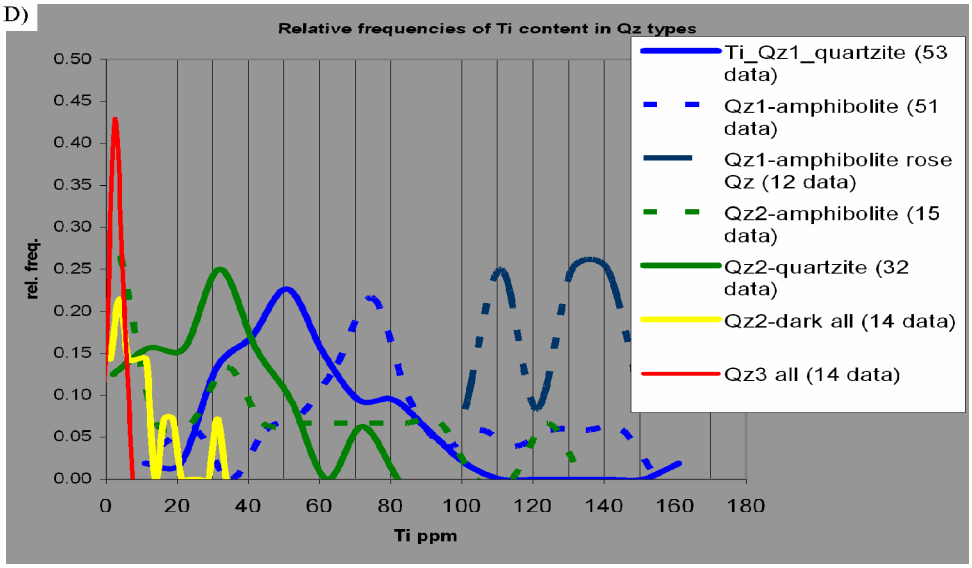

E)

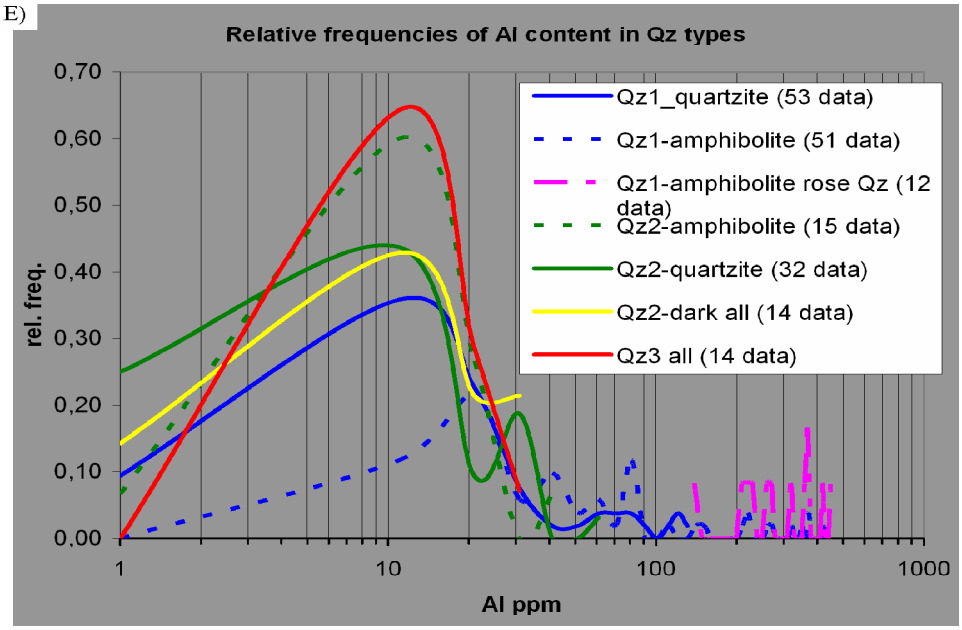

Figure 14: Trace element distribution in quartz. A) All elements shown as bars with mean value ± σ for quartzites (left) and quartz veins and leucosomes in amphibolite (right). B) Plot of Ti vs. Al with bubble size from Boron. C) Linear correlation between Al and B, followed by quartz vein and leucosomes and in amphibolite (blue symbols), but not by Qz1 in quartzite (yellow symbols) . D) Relative frequencies of Ti content in the different quartz types. E) Relative frequencies of Al content in the different quartz types

6 Discussion

This paper focuses on the formation of complex recrystallisation textures in quartz and their relation to fluid flow and deformation. It is demonstrated that the properties of quartz are not constant but vary significantly between quartz types and is related to their defect structure. This has implications for the way we look at the deformation of quartz bearing rocks, i.e. quartz in this study feature variable rheological behaviour. In addition the fluid flow pattern in shearzones is well expressed by the quartzites and inform about mass transfer processes in the crust. In the next sections the role of fluids and the importance of spatial and temporal fluid availability in quartz deformation and recrystallisation are discussed. Another important aspect of this study is the role of fluids in the formation of high purity quartz through quartz recrystallisation. It is demonstrated that quartz oppose recrystallisation at fluid absent conditions although P and T are changing, whereas quartz subjected to aqueous fluids at the same conditions is chemically altered.

6.1 Textural chronology

Four main types of quartz were documented in quartzites and quartz veins in this study (in chronological order):

Qz1: Bright islands surrounded by narrow darker cracks

Qz2: Light grey quartz with the same grey level as the channels in Qz1. Occasionally with oscillatory zoning.

Qz3: Dark grey diffuse channels intersecting Qz1 and Qz2.

Qz4: Black to very dark grey luminescent.

Additionally, different degrees of luminescence quenching characterise each type. Channels in Qz1 match the luminescence level in Qz2. Thus the textures of Qz1 and Qz2 are correlated with the Qz1 grains as the altered protolith grains and Qz2 the newly formed grains. Qz3 textures always intersect Qz1 and Qz2 textures hence are younger. Luminescence quenching textures related to the Qz3 formation comprise several subtypes:

Luminescence quenching (Qz3) occur along grain boundaries between Qz1 and Qz2, and Qz2 and Qz2. This type of Qz3 occurrence is in optical continuity with the Qz2 grains i.e. on the Qz2 side of the grain boundary suggesting that Qz1 was consumed during this process. However, diffuse channels of Qz3 intersects both Qz1 and Qz2, but is more common in Qz2.

6.2 Patterns of recrystallisation

Regardless of the lithological setting, quartz show similar textural types. Qz1 have uneven luminescence with dark channels engulfing brighter islands. Less cracked bright quartz is preserved within minerals such as quartz in the garnet quartz symplectites and dravitic tourmaline in leucosomes in quartz-biotite tourmaline

feldspar gneisses. In the following the processes behind the quartz recrystallisation is discussed. At the end the discussion, a model that may explain the observed pattern of recrystallisation is presented (figure 15).

The presence of aqueous brines in Qz2, the islands texture in Qz1 and the oscillatory zoning in Qz2 imply that brecciation associated with dissolution and re-precipitation is responsible for the formation of Qz2. It was the result of the introduction of aqueous fluids to the dry high grade quartz (Figure 15). Experimental results demonstrate that only small amounts of water are required to greatly lower the creep strength of quartz (e.g. Kronenberg, 1994; Kronenberg et al., 1984) whereas amounts larger than 0.2 wt% will facilitate brecciation of the quartz (e.g. den Brok and Spiers, 1991; Post and Tullis, 1998). Our results confirm these interpretations.

The exact micro-nanoscale role of f_{H2O} in quartz deformation is difficult to access, even in experimentally deformed rocks at high and low f_{H2O}. This is because the changes in intragranular water or hydrogen speciation is impossible to detect although the strength of quartz polycrystalline aggregates is lowered at high water pressures (den Brok et al., 1994; den Brok, 1992; Kronenberg and Wolf, 1990). Therefore, the role of water in deformation of quartz aggregates is complex, and not only intragranular water influence the rock strength but also intergranular water. This interpretation is supported by the fact that quartzites deformed without adding water. With their original saturated intragranular content they have intermediate strengths whereas they have low strengths with added water (e.g. Kronenberg, 1994 and references herein; Kronenberg and Wolf, 1990). Vacuum dried quartzites are strong and primarily deforms by slip on basal planes with dislocation heterogeneous substructures indicative of low recovery rates (e.g. Kronenberg, 1994 p. 161 and references herein). This agrees with the observed increase in luminescence intensity in Qz1 observed in the vicinity of more deformed areas. For example, the coupling between increasing luminescence intensity and changes in subgrain structure from chess board to basal type subgrains in Qz1 grains. This was observed both in quartz veins and quartzites.

In contrast to dry quartzites, dislocation structures in quartz in quartzites that were experimentally deformed under water saturated conditions show homogeneous distributions of both basal and prismatic dislocations and organized dislocation configurations resulting from recovery (e.g. Kronenberg, 1994 p. 161 and references herein). This matches the behaviour of Qz2 and Qz3 which do not show increasing CL-intensity or optical microstructures indicative of recovery toward the high strain zones.

Qz3 behaved far different from Qz2 and Qz1 during thrust related deformation. Qz3 formed subgrains with subgrain rotation eventually leading to new grains with a smaller grain size. In contrast Qz1 and Qz2 mostly behaved brittle or deformed plastically by deformation lamellae. Possibly, the introduction of water in Qz3 not only increased plasticity but also enhanced the local recovery rate (Figure 15) hence facilitating the continuous climb of dislocations during deformation, and lowered work hardening. Initial softening of Qz3 was accomplished by simultaneous cracking and fluid infiltration with the infiltrating aqueous solutions increasing recovery and healing

rates. In this process, the quartz was leached of trace elements. We suggest that this process took place in a system of fine scale cracks associated with larger cracks propagating in a horse tail pattern rather than being the result of diffusive processes (Figure 15). Fluid inclusion studies (paper 2, Sørensen and Larsen, 2007) documents that the fluids related to the formation of Qz3 are brines with a salinity of about 30 wt% NaCl equivalents. Such high salinities provides fluids with a very good wetting capability towards quartz (Watson and Brenan, 1987) hence enabling fluid flow even through narrow sub-microscopic cracks. Therefore, the broad channels may be a result of fluids flowing through a main crack dissolving quartz through a system of finer scale cracks splaying off the main crack hence improving the porosity (Figure 15). The smaller grain size in the Qz3 domains increased the permeability of the quartzites during deformation. Therefore, fluids were focused in high strain ductile areas as they percolated through the fault system simultaneously with the cracking process propagating through less ductile Qz1 and Qz2 (Figure 15). Given this scenario, it appears that both intra- and intergranular water participated in the quartz recovery process on a localised scale sustaining the differential behaviour of the quartz types. This is also supported by TEM observations of the relations between dislocations and nano-inclusions of H_2O in both natural localised high strain domains and in quartzites deformed experimentally at high P_{H2O}. Together, they document that water travelling along grain- and subgrain boundaries play an important role in recovery processes in reducing the work hardening (e.g Kronenberg, 1994). In addition fluid inclusion water in shear zones correlate with localised high shear strains (e.g. Kronenberg et al., 1990; Nakashima et al., 1995). Furthermore, the ductility and recovery rates may be influenced by is the presence and speciation of trace elements in the quartz structure. This is because included trace elements may serve as obstacles for propagating dislocation loops during dislocation glide and obstruct climbing dislocations thus making dislocation glide and recovery through dislocation climb less efficient.

Boundaries between grains of Qz2 commonly are straight and have triple point junctions. Boundaries between Qz1 and Qz2, however, are interlobate-lobate. This suggests that two different processes dominated the geometry control and the two types of grain boundaries. The straight Qz2-Qz2 boundaries are obviously explained by energy minimisation by GBAR (grain boundary area reduction) (e.g. Passchier and Trouw, 2005). Pinning, window, dragging and "left over grain" microstructures (see e.g. Jessell, 1987; Passchier and Trouw, 2005 for definitions) documents that Qz2 grains grew at the expense of Qz1 grains during dynamic recrystallisation. According to existing theories on GBM (grain boundary migration) the GBM process is driven by contrasting dislocation densities between grains i.e. grains with high dislocation densities consume grains with lower dislocation densities in order to minimise the free energy of the system. In our case the high defect concentration in Qz1 is demonstrated by the high and uneven SEM-CL of Qz1 compared to Qz2. The possibility therefore exists that SEM-CL could become an important tool to improve the understanding of the poorly understood GBM process in quartz tectonites.

The relationship between the formation of Qz2 and the addition of aqueous fluids to the quartzites in combination with the observation of aqueous fluid inclusions decorating the irregular boundaries between Qz1 and Qz2 suggest that water travelling along grain boundaries assisted the GBM process in our samples.

The textures of Qz3 intersect Qz1 and Qz2. Because the formation of Qz3 relates to the formation of muscovite and decomposition of biotite to poikiloblastic muscovite, it is implied that Mg and Fe was mobilised from the biotites in the quartzites at the same time as quartz recrystallised to form Qz3. This suggests the action of an aqueous fluid capable of mobilising Fe and Mg from the Biotite, because no other phases are present next to the muscovite grains that otherwise could have consumed the available Mg and Fe. In addition the geometry of the Qz3 textures resembles a fluid channel texture following grain boundaries or intersecting grains in a fingering pattern. Also the clear relationship between aqueous brines and Qz3 imply that Qz3 must relate to the introduction of an aqueous fluid (paper 2, Sørensen and Larsen, 2007). Apparently these brine fluids were capable of both infiltrating quartz and also of changing the quartz properties. Qz3 channels are more common in Qz2 than in Qz1. This may relate to different fluid propagation properties in the two different quartz types. If the fluid is assumed to propagate through micro-cracks, the different fracturing properties of quartz in relation to the water content may control crack growth and healing (see Kronenberg (1994) and references herein).

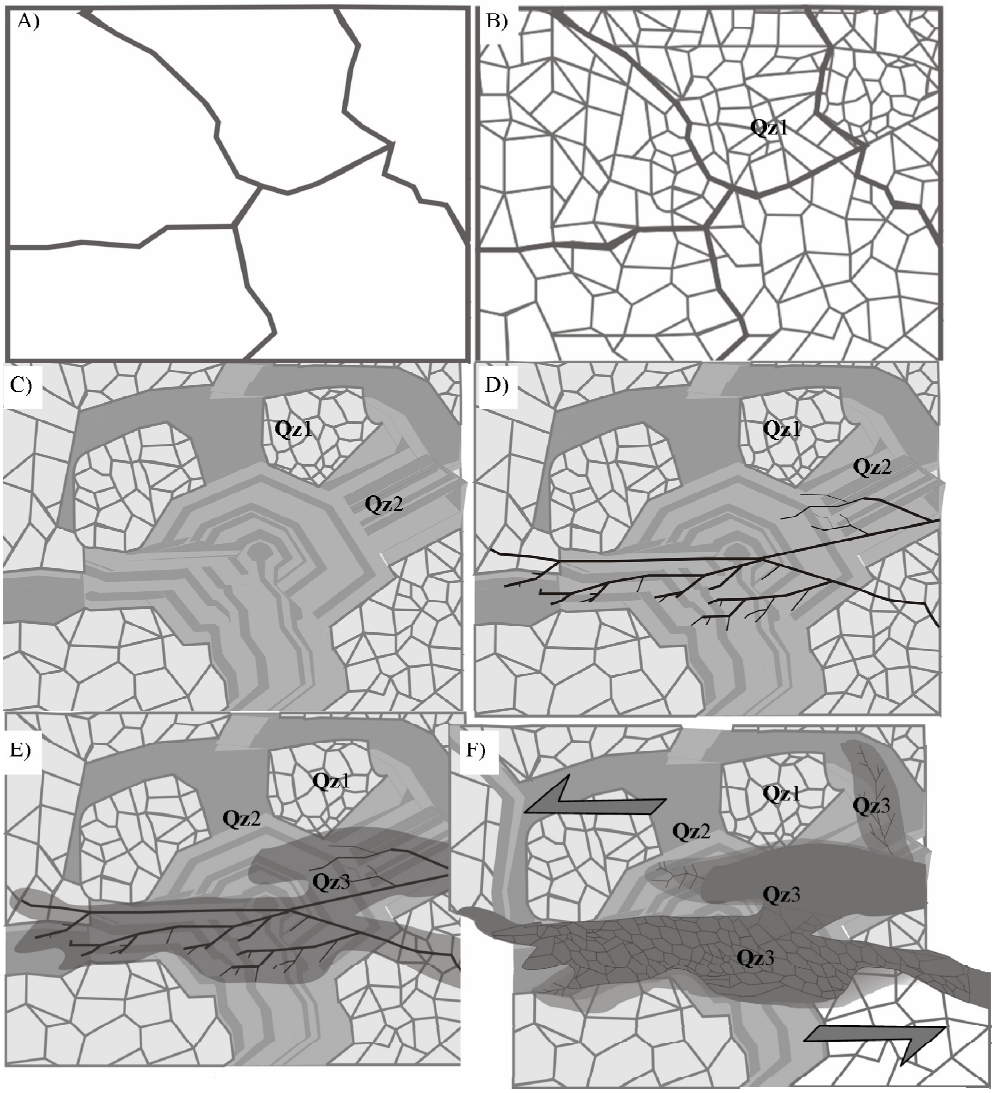

Figure 15: Pattern of recrystallisation as demonstrated by SEM-CL and optical microscopy. A) Homogeneous quartz at high grade conditions. B) Introduction of aqueous fluids under differential stress induced brecciation. C) Quartz dissolved during brecciation precipitates as Qz2, Qz1 being the brecciated old grains. D) Repeated deformation induce fracturing E) Infiltrating aqueous fluids move along the fractures causing recrystallisation (Qz3), but also promoting crack mobility F) The recrystallised quartz (Qz3) behaves more plastic than Qz1 and Qz2 and deform by SGR (subgrain rotation recrystallisation). Continuous fluid flow through the more fine-grained Qz3 domains increase recovery rates and reduce strain hardening. Crack propagation and recrystallisation still continue and the amount of Qz3 increase.

6.3 Trace element distribution and behaviour

Both Qz1 and Qz2 have strongly variable geochemical signatures. The Ti content is variable, but Qz1 has much higher and more variable Al and B contents. Most of both the Al and B in Qz1 come form microscopic inclusions of dumortierite, because the B versus Al trend is almost perfectly linear with a coefficient matching the molar ratio in dumortierite (Figure 14). This is also reflected by the colour variation of Qz1 from blue to pink, with pink quartz being richer in B and Al than blue quartz. Previous studies documented pink coloured dumortierite inclusions in rose quartz (Applin and Hicks, 1987; Goreva et al., 2001). Therefore, it is assumed that mobilisation of B was more intense in relation to the formation of the rose quartz veins. The dumortierite inclusions in quartz grains formed as a result of intergrowth because the strong correlation between B and Al corresponds exactly to that dumortierite (Figure 14).

The difference in SEM-CL between Qz1 and Qz2 probably is a direct or indirect effect of Ti because this element varies most significantly amongst the quartz types (Figure 14). This is also reflected in the SEM-CL spectra of Qz1 and Qz2 that are dominated by possibly Ti-peaks in the quartz lattice, and a peak which probably relate to H_2O and intrinsic defects in the lattice. It is more dominant in Qz2 than in Qz1 (Figure 13). This overall correlation is somewhat clouded by variable content of coarse rutile needles in Qz2, causing Ti variations from 20-100 ppm (Figure 14). However, the average Ti content is much lower in Qz2 than in Qz1 and Qz1 and Qz2 are also easily distinguished in frequency diagrams (figure 14). The Ti-content in Qz2 in quartzites is much lower than the Ti content in Qz2 in quartz veins in the amphibolites. We suggest that the different Ti contents in these two contrasting chemical environments in combination with the stability of rutile and thus simultaneous growth of rutile and quartz caused this difference. This interpretation is supported by the textural correlation between the formation of Qz2 and breakdown of ilmenite to rutile in sample 03bes32 and with the high abundance of coarse rutile needles in Qz2 in quartz veins in amphibolite.

Qz3 is very low in most trace elements including Al, Ti, and B and has low luminescence. Rutile needles are absent in Qz3, probably because titanite, being abundant in the alteration zone surrounding Qz3, is the stable Ti-mineral

In contrast to other trace elements, P is less systematic in going from one quartz type to the next and show variations from 0 ppm to 30 ppm. Either P is very mobile and easily remobilised in and out of the quartz lattice or P is not structurally bound but associated sub microscopic mineral and fluid inclusions.

SEM-CL analysis supports the latter options given that some samples (04bes122) with strongly variable P contents maintain even homogenous SEM-Cl signals.

6.4 Implications for mega shearzone fluid migration

The recrystallisation history stored by the quartzites document the fossil plumbing system that accommodated fluid fluxing from deep seated to shallow parts of the Bamble shear zone complex. Judging from the incoherent geochemistry of Qz1 the

quartz bearing rocks probably experienced high grade metamorphism under variable conditions. The observed differential behaviour of quartz, induced by an infiltrating fluid into a dry protolith uncovers some important aspects of fluid migration in inter-crustal shearzones. It is confirmed that fluids were focused in shearzones is associated with chemical weakening and that large scale mobility of elements occurred. Fe is removed from ilmenite hence facilitating the stability of rutile together with Qz2 and Mg as well as Fe is removed to form muscovite from biotite. These elements are redeposited in other places explaining why ore deposits often occur in the vicinity of shearzones, typically in association with second or third order faults. Therefore, deep crustal shearzones like the Bamble mobile belt serve as fluid conduits providing large scale mass transport. In addition the reduction of grain size in high strain domains increases the number of channel available for fluid transports per volume unit. Once the process of fluid infiltration in localised high strain deformation is initiated, it will probably continue as a self sustained process as long as a fluid supply is available. If however fluid supply ceases, quartz may return to intermediate strength.

6.5 Conclusion and summary

Complex recrystallisation textures in quartz were observed by SEM-CL

- Quartz formed at high metamorphic grades under dry conditions dominated by CO_2-rich fluids, possibly coexisting with brines, underwent localised recrystallisation during cooling and exhumation. Recrystallisation was induced by two main stages of fluid influx.
    - First introduction of aqueous fluids, comprising a mix of CO_2-rich low salinity and CO_2-poor NaCl-KCl-H_2O-CO_2 eutectic salinity brines that provoked brecciation and dissolution re-precipitation of quartz. Quartz types Qz2 and Qz1 bear witness of this process: Qz1 represents relics of old brecciated grains characterised by an uneven luminescence pattern comprising islands with bright luminescence surrounded by darker channels. Qz2 represent quartz that was re-precipitated from the brecciation dissolution process responsible for the formation of Qz1. Luminescence of Qz2 is more even that that of Qz1 but faint oscillatory zoning bear witness to the hydrothermal origin of Qz2. Rutile was the stable Ti-bearing phase when Qz2 formed as documented by the breakdown of ilmenite to rutile in association with Qz2 textures. Coarse rutile needles are common in Qz2 but are more abundant in Qz2 quartz veins in amphibolites than in Qz2 quartzites.
    - Second fluid influx propagated along a feather like system of micro-cracks. Fluids were CO_2 free brines with a good ability to infiltrate the quartz due to low wetting angles facilitated by high salinity brines against quartz also giving a high transport capacity. Fluid infiltration facilitated recrystallisation of quartz (Qz3) in mm wide fluid channels. Qz3 behaved more plastic than Qz1 and Qz2 during deformation and experienced SGR (Sub Grain Rotation recrystallisation). Increased

SEM-Cl intensity in Qz1 toward zones in which Qz3 experienced SGR testify to increased dislocation densities and to strain hardening processes in Qz1. Qz3 is texturally correlated with the breakdown of rutile to titanite. Qz3 correlate with thrust related microstructures. Fluid inclusion studies document the fluid in equilibrium with Qz3 to be brine with 25 wt% NaCl and 6 wt% $CaCl_2$. Fluid inclusion isochore along with the trust related microstructures in relation Qz3 places Qz3 formation during exhumation at 300-400°C, 3-6 kb.

- Several later fluid influxes caused localised quartz recrystallisation along micron-wide micro-cracks (Qz4).

Trace elements in quartz were gradually removed from the quartz lattice during retrograde recrystallisation correlated with luminescence quenching textures.

Ti along with intrinsic and water related defects is probably responsible for the luminescence observed in our samples and undergoes a progressive depletion during retrograde recrystallisation:

- Qz1 is richest in structurally bound Ti.
- Qz2 is lower in structurally bound Ti but contain numerous rutile needles formed as intergrowth because rutile was the stable Ti phase during Qz2 formation. This cause the bulk Ti-content in Qz2 from quartz veins in amphibolite to vary unsystematically because rutile needles were too abundant to be avoided during LA-ICP-MS analyses. Qz2 in quartzite on the contrary gives a constrained average of 32 ppm.
- Qz3 is low in Ti and also in other trace elements. This is partially because of the low abundance of structurally bound trace elements, but the destabilisation of rutile in relation to Qz3 served to produce quartz with a uniform low bulk Ti concentration below 5 ppm.

Our study underlines the importance of fluids on quartz rheology. This is demonstrated by the differential behaviour of Qz1, Qz2 and Qz3 during deformation. During uplift Qz3 deformed plastically and recovered by SGR. At the same time Qz1 experienced strain hardening caused by accumulation of dislocations demonstrated by increased cathodoluminescence intensity. In agreement with experimental studies we infer that the increased plasticity and recovery rate in Qz3 was caused by increased H_2O content in the fluid. This interpretation is substantiated by the record of fluid inclusion in Qz3 by Sørensen and Larsen (2007, paper 2). However, it is also suggested that the trace elements in quartz may affect the rheological properties as trace elements in the quartz lattice may obstruct dislocation glide as well as dislocation climb hence promoting strain hardening.

Grain boundary geometries are also partially controlled by the trace element contents. Qz1-Qz2 grain boundaries are interlobate-lobate with microstructures. Qz2

grew at the expense of Qz1 during GBM, whereas Qz2-Qz2 boundaries are straight with common triple junctions implying static recrystallisation dominated by GBAR.

Our results demonstrate the in the importance of narrow fluid pathways in quartzite lithologies in shearzones. Areas highly affected by metasomatism induced by infiltrating fluid are juxtaposed with apparently unaffected areas millimetres or microns away.

Acknowledgements

Arild Monsøy and Kjetil Eriksen at the thin section laboratory at IGB, NTNU are thanked for patiently having prepared dozens of carefully polished thin sections. Belinda Flem and Øyvin Skår at NGU are acknowledged for their assistance with LA-HR-ICP-MS analyses at NGU. John Rasmus Leinum, Tor Arrild Nilsen, Kari Moen and Jarle Hjelen at NTNU are acknowledged for helping out with the SEM-equipment at NTNU. This study was financed by the NFR grant to the Strategic University Program entitled "The value chain from mineral deposit to beneficiated product with emphasis on quartz".

References

Applin, K.R. and Hicks, B.D., 1987. Fibers of dumortierite in quartz. American Mineralogist, 71: 786-794.

Cameron, E.M., 1993. Reintroduction of gold, other chalcophile elements and LILE during retrogression of depleted granulite, Tromoy, Norway. Lithos, 29(3-4): 303-309.

Cameron, E.M., Cogulu, E.H. and Stirling, J., 1993. Mobilization of gold in the deep crust - Evidence from mafic intrusions in the Bamble Belt, Norway. Lithos, 30(2): 151-166.

Colivine, A.C. et al., 1984. An intergrated model for the origin of Archean lode gold deposits: Ontario. Geological Survey Open-file Report, 5524, 98 pp.

den Brok, B., Meinecke, J. and Roeller, K., 1994. FTIR determination of intragranular water content in quartzites experimentally deformed with and without added water in the ductile deformation field. Journal of Geophysical Research, B, Solid Earth and Planets, 99: 19821-19828.

den Brok, B. and Spiers, C.J., 1991. Experimental evidence for water weakening of quartzite by microcracking plus solution-precipitation creep. Journal of the Geological Society of London, 148: 541-548.

den Brok, S.W.J., 1992. An experimental investigation into the effect of water on the flow of quartzite. Geologica Ultraiectina, 95. Rijkuniversiteit, Mineralogisch-geologisch Instituut, Utrecht, Netherlands, 177 pp.

Flem, B., Larsen, R.B., Grimstvedt, A. and Mansfeld, J., 2002. In situ analysis of trace elements in quartz by using laser ablation inductively coupled plasma mass spectrometry. Chemical Geology, 182(2-4): 237-247.

Goetze, J., 2000. Cathodoluminescence in applied geosciences. In: M. Pagel, V. Barbin, P. Blanc and D. Ohnenstetter (Editors), Cathodoluminescence in geosciences. Springer. Berlin, Federal Republic of Germany. 2000.

Goetze, J., Ploetze, M., Graupner, T., Hallbauer, D.K. and Bray, C.J., 2004. Trace element incorporation into quartz; a combined study by ICP-MS, electron spin resonance, cathodoluminescence, capillary ion analysis, and gas chromatography. Geochimica et Cosmochimica Acta, 68(18): 3741-3759.

Goetze, J., Ploetze, M. and Trautmann, T., 2005. Structure and luminescence characteristics of quartz from pegmatites. American Mineralogist, 90(1): 13-21.

Goetze, J., Plotze, M. and Habermann, D., 2001. Origin, spectral characteristics and practical applications of the cathodolumimescence (CL) of quartz - a review. Mineralogy and Petrology, 71(3-4): 225-250.

Goreva, J.S., Ma, C. and Rossman, G.R., 2001. Fibrous nanoinclusions in massive rose quartz: The origin of rose coloration. American Mineralogist, 86: 466-472.

Griggs, D.T. and Blacic, J.D., 1965. Quartz; Anomalous weakness of synthetic crystals. Science, 147(3655): 292-295.

Groves, D.I. et al., 1992. Sub-greenshist- to granulite-hosted Archean lode gold deposits of the Yilgarn Craton: A depositional continuum from deep -sourced hydrothermal fluids in crustal-scale plumbing systems. In: J.E. Glover and S.E. Ho (Editors), The Archean: Terrains, processes and metallogeny. Geology Department UNiversity Extension 22. University of Western Australia Publication, pp. 325-337.

Harlov, D.E., 2000. Titaniferous magnetite-ilmenite thermometry and titaniferous magnetite-ilmenite-orthopyroxene-quartz oxygen barometry in granulite facies gneisses, Bamble sector, SE Norway; implications for the role of high-grade CO_2-rich fluids during granulite genesis. Contributions to Mineralogy and Petrology 139: 180-197

Jessell, M.W., 1987. Grain-boundary migration microstructures in a naturally deformed quartzite. Journal of Structural Geology, 9(8): 1007-1014.

Knudsen, T.L., 1996. Petrology and geothermobarometry of granulite facies metapelites from the Hisøy-Torungen area, South Norway; new data on the Sveconorvegian P-T-t path of the Bamble sector. Journal of Metamorphic Geology, 14(3): 267-287.

Kohlstedt, D.L., Evans, B. and Mackwell, S.J., 1995. Strength of the lithosphere; constraints imposed by laboratory experiments. Journal of Geophysical Research, B, Solid Earth and Planets, 100(9): 17,587-17,602.

Kronenberg, A.K., 1994. Hydrogen speciation and chemical weakening of quartz. In: P.J. Heaney, C.T. Prewitt and G.V. Gibbs (Editors), Silica; physical behavior, geochemistry and materials applications. Reviews in Mineralogy.

Mineralogical Society of America, Washington, DC, United States, pp. 123-176.
Kronenberg, A.K., Kirkby, S.H., Aines, R.D. and Rossman, G.R., 1986. Solubility and Diffusional uptake of hydrogen in quartz at high water pressures: implication for hydrolytic weakening Journal of Geophysical Research, B, Solid Earth and Planets, 91: 12723-12744.
Kronenberg, A.K., Segall, P. and Wolf, G.H., 1990. Hydrolytic weakening and penetrative deformation within a natural shear zone. In: A.G. Duba, W.B. Durham, J.W. Handin and F. Wang Herbert (Editors), The brittle-ductile transition in rocks. Geophysical Monograph. American Geophysical Union, Washington, DC, United States, pp. 21-36.
Kronenberg, A.K. and Wolf, G.H., 1990. Fourier transform infrared spectroscopy determinations of intragranular water content in quartz-bearing rocks; implications for hydrolytic weakening in the laboratory and within the Earth. Tectonophysics, 172(3-4): 255-271.
Kronenberg, A.K., Wolf, G.H. and Segall, P., 1984. Variations in intragranular water within a strain gradient; FTIR traverse across a ductile shear zone, AGU 1984 fall meeting. Eos, Transactions, American Geophysical Union. American Geophysical Union, Washington, DC, United States, pp. 1098.
Landtwing, M.R. and Pettke, T., 2005. Relationships between SEM-cathodoluminescence response and trace-element composition of hydrothermal vein quartz. American Mineralogist, 90(1): 122-131.
McCuaig, T.C. and Kerrich, R., 1998. P-T-t-deformation-fluid characteristics of lode gold deposits: Evidence from alteration systematics. Ore Geology reviews, 12: 381-453.
Müller, A., Wiedenbeck, M., Van den Kerkhof, A.M., Kronz, A. and Simon, K., 2003. Trace elements in quartz; a combined electron microprobe, secondary ion mass spectrometry, laser-ablation ICP-MS, and cathodoluminescence study. European Journal of Mineralogy, 15(4): 747-763.
Muto, J., Nagahama, H. and Hashimoto, T., 2004. Microinfrared reflection spectroscopic mapping: application to the detection of hydrogen-related species in natural quartz. Journal of Microscopy, 216: 222-228.
Muto, J., Nagahama, H. and Hashimoto, T., 2005. Water distribution in dynamically recrystallized quartz grains: cathodoluminescence and micro-infrared spectroscopic mappings. In: L. Burlin and D. Bruhn (Editors), Microstructural Evolution and Physical Properties in High-strain Zones. GSL Special Publications. Geological Society of London.
Nakashima, S. et al., 1995. Infrared microspectroscopy analysis of water distribution in deformed and metamorphosed rocks. In: C.J. Spiers and T. Takeshita (Editors), Influence of fluids on deformation processes in rocks. Tectonophysics. Elsevier, Amsterdam, Netherlands, pp. 263-276.
Nesbit, B.E. and Muehlenbachs, K., 1989. Geology, Geochemistry, and genesis of mesothermal lode gold deposits of the Canadian Cordillera: Evidence for ore

formation from evolved meteoric water. In: R.R. Keays, W.R.H. Ramsay and D.I. Groves (Editors), The geology of gold deposits: The perspektive in 1988. Economic Geology Monograph 6, pp. 553-563.

Nesbit, B.E., Murowchcik, J.B. and Muehlenbachs, K., 1986. Dual origins of lode gold deposits in the Canadian Cordillera. Geology, 14: 506-509.

Nijland, T.G., Liauw, F., Visser, D., Maijer, C. and Senior, A., 1993a. Metamorphic petrology of the Froland corundum-bearing rocks; the cooling and uplift history of the Bamble sector, South Norway. Bulletin - Norges Geologiske Undersokelse, 424: 51-63.

Nijland, T.G. and Maijer, C., 1993. The regional amphibolite to granulite facies transition at Arendal, Norway; evidence for a thermal dome. Neues Jahrbuch fuer Mineralogie Abhandlungen, 165: 191-221.

Nijland, T.G., Maijer, C., Senior, A. and Verschure, R.H., 1993b. Primary sedimentary structures and composition of the high-grade metamorphic Nivelda quartzite complex (Bamble, Norway), and the origin of nodular gneisses. Proceedings of the Koninklijke Nederlandse Akademie van Wetenschappen (1990), 96(2): 217-232.

Nijland, T.G. and Touret, J.L.R., 2001. Replacement of graphic pegmatite by graphic albite-actinolite-clinopyroxene intergrowths (Mjavatn, southern Norway). European Journal of Mineralogy, 13(1): 41-50.

Nijland, T.G., Touret, J.L.R. and Visser, D., 1998. Anomalously low temperature orthopyroxene, spinel, and sapphirine occurrences in metasediments from the Bamble amphibolite-to-granulite facies transition zone (South Norway); possible evidence for localized action of saline fluids. Journal of Geology, 106(5): 575-590.

Passchier, C.W. and Trouw, R.A.J., 2005. Microtectonics. 2 ed. Springer. Berlin, Federal Republic of Germany. Pages: 366. 2005.

Post, A. and Tullis, J., 1998. The rate of water penetration in experimentally deformed quartzite; implications for hydrolytic weakening. In: M. Chester Fred, T. Engelder and T. Shimamoto (Editors), Rock deformation; the Logan volume. Tectonophysics. Elsevier, Amsterdam, Netherlands, pp. 117-137.

Post, A.D., Tullis, J. and Yund, R.A., 1996. Effects of chemical environment on dislocation creep of quartzite. Journal of Geophysical Research, B, Solid Earth and Planets, 101(10): 22,143-22,155.

Sibson, R.H., Robert, F. and Poulsen, K.H., 1988. High-angle reverse faults, fluid pressure cyckling, and mesothermal gold-quartz deposits. Geology, 16: 551-555.

Sørensen, B.E., 2007. Metamorphic refinement of quartz under influence of fluids during exhumation with reference to the metamorphic/metasomatic evolution observed in amphibolites - a detailed field, microtectonic and geochemical study from the Bamble sector, South Norway. PhD Thesis (in prep.) Thesis, NTNU, Trondheim.

Sørensen, B.E. and Larsen, R.B., 2007. Paper2: The fluid evolution of the Froland area in the Bamble sector from peak P-T through cooling and uplift: implications for retrograde mineral paragenesis and PT evolution of the Bamble sector. In: B.E. Sørensen (Editor), Metamorphic refinement of quartz under influence of fluids during exhumation with reference to the metamorphic/metasomatic evolution observed in amphibolites - a detailed field, microtectonic and geochemical study from the Bamble Sector, South Norway. PhD Thesis, Department of Geology and Mineral Resources Engineering, NTNU Trondheim.

Sørensen, B.E., Larsen, R.B. and Austrheim, H., 2007. Paper3: Metasomatic evolution of the Froland amphibolites during cooling and uplift - textural observations and geochemical evolution of hydrous minerals. In: B.E. Sørensen (Editor), Metamorphic refinement of quartz under influence of fluids during exhumation with reference to the metamorphic/metasomatic evolution observed in amphibolites - a detailed field, microtectonic and geochemical study from the Bamble Sector, South Norway. PhD Thesis, Department of Geology and Mineral Resources Engineering, NTNU Trondheim.

Touret, J., 1968. The Precambrian metamorphic rocks around the Lake Vegår (Aust-Agder, southern Norway). Norges Geologiske Undersøkelse, 257, 45 pp.

Touret, J., 1971. Le faciès granulite en Norvège méridionale II Les inclusions fluides. Lithos, 4: 423-436.

Touret, J., 1985. Fluid regime in southern Norway: the record of fluid inclusions. In: A.C. Tobi and J. Touret (Editors), The deep Proterozoic crust in the North Atlantic Provinces NATO ASI Ser. Ser. C: Math. Phys. Sci., pp. 517-549.

Touret, J. and Olsen, S.N., 1985. Fluid inclusions in migmatites. In: J.R. Ashworth (Editor), Migmatites. Shiva, Glasgow, pp. 265-288.

Tullis, J., 2002. Deformation of Granitic Rocks: Experimental Studies and Natural Examples In: S.-i. Karato and H.-R. Wenk (Editors), Plastic Deformation in Minerals and Rocks. Reviews in MIneralogy. MSA.

Tullis, J. and Yund, R.A., 1989. Hydrolytic weakening of quartz aggregates; the effects of water and pressure on recovery. Geophysical Research Letters, 16(11): 1343-1346.

Van den Kerkhof, A.M., Kronz, A., Simon, K. and Scherer, T., 2004. Fluid-controlled quartz recovery in granulite as revealed by cathodoluminescence and trace element analysis; Bamble sector, Norway. Contributions to Mineralogy and Petrology, 146(5): 637-652.

Wark, D. and Watson, E.B., 2006. TitaniQ: a titanium-in-quartz geothermometer Contributions to Mineralogy and Petrology, 152(6): 743-754.

Watson, E.B. and Brenan, J.M., 1987. Fluids in the Lithosphere, 1. Experimentally determined wetting characteristics of CO_2-H_2O fluids and their implications for fluid transport, host-rock physical properties, and fluid inclusion formation. Earth Planet Scientific Letters, 85: 496-515.